



Review – Frank Reith memorial issue

The photogeochemical cycle of Mn oxides on the Earth's surface

Anhuai Lu*†, Yan Li†, Feifei Liu, Yuwei Liu, Huan Ye, Ziyi Zhuang, Yanzhang Li, Hongrui Ding and Changqiu Wang

Beijing Key Laboratory of Mineral Environmental Function, School of Earth and Space Sciences, Peking University, Beijing 100871, PR China; and The Key Laboratory of Orogenic Belts and Crustal Evolution, School of Earth and Space Sciences, Peking University, Beijing 100871, PR China

Abstract

Manganese (Mn) oxides have been prevalent on Earth since before the Great Oxidation Event and the Mn cycle is one of the most important biogeochemical processes on the Earth's surface. In sunlit natural environments, the photochemistry of Mn oxides has been discovered to enable solar energy harvesting and conversion in both geological and biological systems. One of the most widespread Mn oxides is birnessite, which is a semiconducting layered mineral that actively drives Mn photochemical cycling in Nature. The oxygen-evolving centre in biological photosystem II (PSII) is also a Mn-cluster of Mn_4CaO_5 , which transforms into a birnessite-like structure during the photocatalytic oxygen evolution process. This phenomenon draws the potential parallel of Mn-functioned photoreactions between the organic and inorganic world. The Mn photoredox cycling involves both the photo-oxidation of Mn(II) and the photo-reductive dissolution of Mn(IV/III) oxides. In Nature, the occurrence of Mn(IV/III) photoreduction is usually accompanied with the oxidative degradation of natural organics. For Mn(II) oxidation into Mn oxides, mechanisms of biological catalysis mediated by microorganisms (such as *Pseudomonas putida* and *Bacillus* species) and abiotic photoreactions by semiconducting minerals or reactive oxygen species have both been proposed. In particular, anaerobic Mn(II) photo-oxidation processes have been demonstrated experimentally, which shed light on Mn oxide emergence before atmospheric oxygenation on Earth. This review provides a comprehensive and up-to-date elaboration of Mn oxide photoredox cycling in Nature, and gives brand-new insight into the photochemical properties of semiconducting Mn oxides widespread on the Earth's surface.

Keywords: Mn oxides, birnessite, semiconducting minerals, photogeochemical cycling, mineral evolution

(Received 21 November 2020; accepted 28 January 2021; Accepted Manuscript published online: 1 February 2021;

Guest Associate Editor: Janice Kenney)

Introduction

Manganese oxides have long been spread ubiquitously on Earth, from the Mn deposits in Precambrian strata (Roy, 1997), to the Mn nodules spread over the sea floor (Bauman, 1976; Jiang *et al.*, 2007) and the Mn-enriched rock or soil surface coatings (Bauman, 1976; Post, 1999; McKeown and Post, 2001; Dorn, 2007; Nash *et al.*, 2007; Xu *et al.*, 2018; Lu *et al.*, 2019a). Manganese oxides are diverse in both phase and structure and comprise mixed Mn(IV/III/II) valence states with layered, tunnelled or spinel-type structures (Post, 1999; Johnson *et al.*, 2016). In Nature, Mn oxides are widespread in coatings on the upper surface of rocks and soils (Lu *et al.*, 2019a), where the dominant phase in the coatings is birnessite – a layered mineral with Mn (or O) vacancy and adsorbed cations (Post, 1999; McKeown and Post, 2001; Villalobos *et al.*, 2003; Webb *et al.*, 2005; Villalobos *et al.*, 2006; Lu *et al.*, 2019a; Xu *et al.*, 2019; Elmi, C. *et al.*, 2021). As a semiconducting mineral, birnessite shows outstanding photocatalytic reactivity (Sherman, 2005; Ling *et al.*, 2017; Lu *et al.*, 2019a) and, as revealed by theoretical calculations, the electronic structure of birnessite is sensitive to Mn (or

O) vacancy abundance as well as the metal sorption sites (Kwon *et al.*, 2008, 2009; Li *et al.*, 2019a). These effects further impact the photocatalytic performance of birnessite in various photoreactions, mainly during birnessite self-reduction (Li *et al.*, 2019a) or reduction by organics (Sunda *et al.*, 1983; Waite *et al.*, 1988; Sunda and Huntsman, 1990) as well as water photocatalytic oxidation (Sherman, 2005; Marafatto *et al.*, 2015). Notably, the oxygen-evolving centre (OEC) in biological photosystem II (PSII) as Mn_4CaO_5 is structurally similar to birnessite (Hocking *et al.*, 2011; Robinson *et al.*, 2013; Yang *et al.*, 2015), which draws the interesting parallel of the key functioning components in water oxidation and oxygen evolution between the organic and inorganic world. As a counterpart to Mn reduction, the oxidation of Mn(II) to form natural Mn oxides has been proposed through catalytic oxidation by fungi and bacteria (Northup *et al.*, 2010), or light-driven photo-oxidation by co-present semiconducting minerals (Madden and Hochella, 2005; Xu *et al.*, 2018; Xu *et al.*, 2019). More recently, the photo-stimulated anaerobic formation of Mn oxides has been observed through the photo-oxidation of Mn(II) carbonate minerals (Liu *et al.*, 2020; Lyons *et al.*, 2020) or biomineralisation mediated by anoxygenic photosynthetic microorganisms (Daye *et al.*, 2019; Lyons *et al.*, 2020). These studies have implications on light-dependent Mn(II) oxidation, and Mn oxides emergence, prior to the Great Oxidation Event on Earth, especially in oceanic euphotic zones. During the oxidative formation of birnessite, sorption sites of heavy metals and the fine structure of birnessite will constantly interact

*Author for correspondence: Anhuai Lu, Email: ahlu@pku.edu.cn

†Equal contributions

This paper is part of a thematic set in memory of Frank Reith.

Cite this article: Lu A., Li Y., Liu F., Liu Y., Ye H., Zhuang Z., Li Y., Ding H. and Wang C. (2021) The photogeochemical cycle of Mn oxides on the Earth's surface. *Mineralogical Magazine* 85, 22–38. <https://doi.org/10.1180/mgm.2021.10>

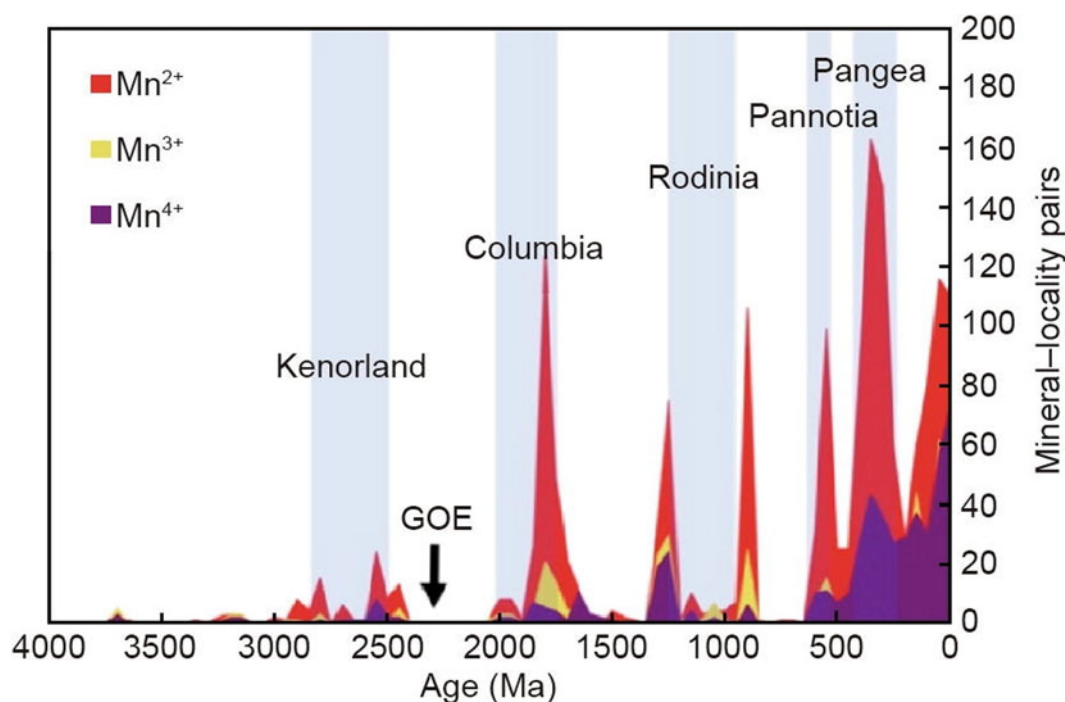


Fig. 1. Evolution of average oxidation state of Mn-bearing minerals on the Earth (from Hazen *et al.*, 2019). GOE – Great Oxidation Event.

with each other, which ultimately determines the biogeochemical cycle of Mn together with heavy metals.

This review first looks back on the mineral evolution processes of Mn oxides throughout geological history and the vast occurrence of Mn oxides in various modern natural settings. Notably, Mn coatings widespread on the Earth's surface, together with its remarkable performance of photon-to-electron conversion under solar irradiation are highlighted. Further, the effect of Mn (or O) vacancies and metal cation sorption on the electronic structure and photocatalytic activity of Mn oxides as revealed by density function theory are summarised. Manganese oxides participate actively in photocatalytic redox cycling on the Earth's surface, involving both the photo-oxidation of Mn(II) and the photoreductive dissolution of Mn oxides. During these processes, heavy metal sorption/desorption, organic oxidation, and even water splitting and oxygen evolution can occur. This study provides novel insights into the photogeochemical cycling of natural Mn oxides as well as its environmental implications.

Natural occurrence of Mn oxides

Coevolution of Mn valence states within the geosphere and biosphere

Mineral ecology of manganese

Manganese is concentrated mainly in the Earth's mantle (~1200 ppm; Turekian and Wedepohl, 1961; Jackson and Dasgupta, 2008), whereas the average content of Mn in the Earth's crust is 950 ppm (Taylor, 1964). The oxidation state of Mn-bearing minerals has increased in an episodic manner from II to IV since 2.5 Ga to the present (Hazen *et al.*, 2019). The majority of Mn oxides with high-valence Mn appeared after the major oxidation events (Hazen *et al.*, 2019; Fig. 1). The highest and lowest valence states of Mn oxides observed in Nature are IV and II, respectively (Owen and Bricker, 1965). Manganese

deposits were produced mainly in the Precambrian such as Moanda, Gabon (Gauthier-Lafaye *et al.*, 1996) and Hunan Province, South China (Yu *et al.*, 2020), while high-quality Mn oxide ores were enriched in the Ordovician, Carboniferous and Quaternary such as at Molango, Mexico (Martino, 1986). Manganese ore is generally formed during deep sea sedimentation, where the main ore is manganese carbonates such as rhodochrosite (Roy, 2006).

There are three kinds of common Mn oxides, which have different arrangements of Mn–O octahedra, i.e. tunnel structures (pyrolusite, ramsdellite, nsutite, hollandite, romanèchite, todorokite and manganite); layered structures (lithiophorite, chalcophanite, birnessite and vernadite); and spinel-like structures (hausmannite) (Table 1). Pyrolusite (β -MnO₂) and ramsdellite usually occur in low-temperature hydrothermal deposits (Post, 1999). Nsutite (γ -MnO₂) is the intergrowth of pyrolusite and ramsdellite structures (Zwicker *et al.*, 1962; Turner and Bruseck, 1983), which forms metasomatic veins in Mn carbonate rocks. These Mn minerals also transform into each other during geological evolution (Post, 1999).

Recent studies have demonstrated that rocks with a dark Mn-rich varnish are generally found on the sunlit side of landforms, and Mn-poor rocks commonly occur on the shaded side (Nealson, 2015; Schindler and Dorn, 2017; Lu *et al.*, 2019a). In addition, the growth rate of Mn-rich coatings was found to be much faster in high-UV flux or photic environments (Krinsley *et al.*, 2009; Koschinsky and Hein, 2017). This phenomenon implies a close relationship between the formation of supergene Mn oxides and solar light (Lu *et al.*, 2019a).

Manganese mineral evolution

According to stellar nucleosynthesis theory (the B²FH theory), Mn formed 400 million years after the Big Bang (Burbidge *et al.*, 1957; Burbidge, 2008). After the formation of the Earth, the sedimentary

Table 1. Classification of manganese (oxyhydr)oxides and structure types.

Structure / Mineral name	Chemical formula
Tunnel structure	
Pyrolusite	$\beta\text{-MnO}_2$
Ramsdellite	MnO_2
Nsutite	$\gamma\text{-MnO}_2$
Hollandite	$R_{0.8-1.5}(\text{Mn}^{\text{IV}}, \text{Mn}^{\text{III}})_8\text{O}_{16}$ $R = \text{Ba, Pb, K or Na}$
Romanèchite	$\text{Ba}_{0.66}(\text{Mn}^{\text{IV}}, \text{Mn}^{\text{III}})_5\text{O}_{10} \cdot 1.34\text{H}_2\text{O}$
Todorokite	$(\text{Ca, Na, K})_{0.3-0.5}[\text{Mn}^{\text{IV}}, \text{Mn}^{\text{III}}, \text{Mg}]_6\text{O}_{12} \cdot 3-4.5\text{H}_2\text{O}$
Manganite	$\gamma\text{-MnOOH}$
Feitknechtite	MnOOH
Layered structure	
Lithiophorite	$\text{LiAl}_2[(\text{Mn}^{\text{IV}}, \text{Mn}^{\text{III}})]_2\text{O}_6(\text{OH})_6$
Chalcophanite	$\text{ZnMn}_3\text{O}_7 \cdot 3\text{H}_2\text{O}$
Birnessite	$(\text{Na, Ca, Mn}^{\text{II}})\text{Mn}_7\text{O}_{14} \cdot 2.8\text{H}_2\text{O}$
Vernadite	$\text{MnO}_2 \cdot n\text{H}_2\text{O}$
Pyrochroite	$\text{Mn}(\text{OH})_2$
Spinel structure	
Hausmannite	$\text{Mn}^{\text{II}}\text{Mn}^{\text{III}}\text{O}_4$
Halite structure	
Manganosite	MnO

geochemistry of Mn has been controlled primarily by redox reaction, and is influenced by multiple Earth processes such as changing sea level and climate (Roy, 2006). The high oxidation states Mn(III) and Mn(IV) exist in insoluble (oxyhydr)oxides in the oxidising environment and the low oxidation state (Mn(II)) is more easily dissolved in the anoxic waters (Johnson *et al.*, 2016). The early Archean atmosphere and hydrosphere system were extremely oxygen deficient (Lyons, 2014). The super mantle plume and high-temperature hydrothermal activities from mantle heat flux introduced a large amount of soluble Mn(II) into the anoxic ocean (Kasting, 1993). From the Archean to the Proterozoic, the rapid burial of organic matter and the gradual reduction of reducing gases in the oxidised mantle resulted in the decrease of an oxygen sink and the increase of photosynthetic oxygen production (Roy *et al.*, 2006). Approximately 2.75 Ga, ‘whiffs’ of oxygen (Kaufman *et al.*, 2007; Frei *et al.*, 2009; Lyons *et al.*, 2014), possibly contributed to the initial widespread formation of Mn oxides (Fig. 1; Hazen *et al.*, 2019). The main Mn minerals in these Archean deposits are still kutnohorite ($\text{CaMn}(\text{CO}_3)_2$), rhodochrosite (MnCO_3) and braunite ($\text{Mn}_6^{\text{III}}\text{Mn}^{\text{II}}\text{O}_8\text{SiO}_4$) (Johnson *et al.*, 2016). In the period 2.4–2.06 Ga, the initial increase of O_2 in the atmosphere did not bring about the complete oxidation of the global ocean, but instead only oxidised surface waters (Reinhard *et al.*, 2009; Kendall *et al.*, 2010). Manganese oxides in this environment could not be dominant; Mn would have a tendency to be reduced and precipitate carbonates due to the degradation of organics. After 2.06 Ga, many Mn-bearing deposits were found to have increased episodes, in which the source of dissolved Mn(II) was crucial (Roy, 2006). Some tectonic activities and glacioeustatic sea-level changes would have enhanced the weathering of silicates

and improve the concentration of dissolved Mn(II), giving rise to its precipitation as carbonates in Neoproterozoic, early Palaeozoic and early Jurassic (Beukes, 1996; Böttcher and Huckried, 1997; Roy, 2006). Large Mn oxide deposits after the Proterozoic (e.g. Cretaceous age) were produced by transgression–regression in a greenhouse climate (Fan *et al.*, 1992).

The average oxidation state of Mn increased with the enhancement of atmospheric oxygen content, which can be divided into five stages (Holland, 2006) (Table 2). In the first stage (4.60–2.45 Ga), the O_2 content of the Archean atmosphere was generally less than $\sim 10^{-5}$ present atmospheric level (PAL) and the average oxidation state of Mn was 2–2.5 (e.g. rhodochrosite). In the second stage of the Columbia supercontinent period (2.45–1.85 Ga), the free oxygen content in the atmosphere rose sharply to between 0.02 and 0.04 atm due to the Great Oxidation Event, and the average oxidation state of Mn was 2.2–2.6 (Hazen *et al.*, 2019). The main Mn minerals at that time, for example in the Koegas subgroup and Hotazel formation in South Africa, were braunite, kutnohorite, rhodochrosite, Mn-rich siderite and Mn-rich calcite (Cairncross and Beukes, 2013). In the third stage during the Rodinia supercontinent period (1.85–0.85 Ga), there was no significant change in atmospheric oxygen content and the average oxidation state of Mn was 2–2.8. Deposits such as Santa Cruz in the Jacadigo Basin, Brazil, were formed where the main Mn minerals are braunite, rhodochrosite, kutnohorite and carypillite (Piacentini *et al.*, 2013). In the fourth stage during the Pannotia supercontinent period (0.85–0.54 Ga), the atmospheric oxygen content rose to a value of more than 0.2 atm, which resulted in three ice ages (snowball Earth events; Hoffman and Schrag, 2010) with the Mn average oxidation state of 2.3–2.6. In the fifth stage (0.54 Ga to present), the oxygen content in the atmosphere rose higher to the maximum value of 0.3 atm in the Carboniferous, and then returned to the present value 0.2 atm. During the Carboniferous, the average oxidation state of Mn was 2.5–3 and in deposits such as those in the Sea of Japan, the main Mn minerals are magnesite, siderite, Mn-rich calcite/kutnohorite and Ca-rich rhodochrosite (Matsumoto, 1992). Modern Mn deposits are mainly superegne or marine sedimentary deposits (Roy, 2006), where the Mn minerals are mainly tetravalent (Maynard, 2010; Johnson *et al.*, 2016).

Mn₄CaO₅ and water oxidation reactions

Water oxidation is one of the most important reactions in Nature (Hocking *et al.*, 2011). The origin of water oxidation can be traced back to the late Archean, in which cyanobacteria have served as the earliest important producers of O_2 by photosynthesis and may produce trace amounts of oxygen, accumulating in some local environments (Lalonde *et al.*, 2015; Lyons *et al.*, 2014). Interestingly, studies have shown that Mn oxide, a by-product of photosynthesis, already existed before the emergence of cyanobacteria (Johnson *et al.*, 2013). That is, the photocatalytic oxygen production by layered Mn oxides is possibly the embryonic form

Table 2. Five stages of Mn average oxidation state changing with atmospheric oxygen content.

Stage	I	II	III	IV	V
Time envelope	4.60–2.45 Ga	2.45–1.85 Ga	1.85–0.85 Ga	0.85–0.54 Ga	the last 0.54 Ga
Atmospheric O_2 level	$< \sim 10^{-5}$ PAL	10–20% PAL	20% PAL	20–100% PAL	175–100% PAL
Average oxidation state	2–2.5	2.2–2.6	2–2.8	2.3–2.6	2.5–3.0
Events	—	Great Oxidation Event	Canfield Ocean	Snowball Earth	Oceanic anoxic events
Supercontinents	Kenorland	Columbia	Rodinia	Pannotia	Pangea

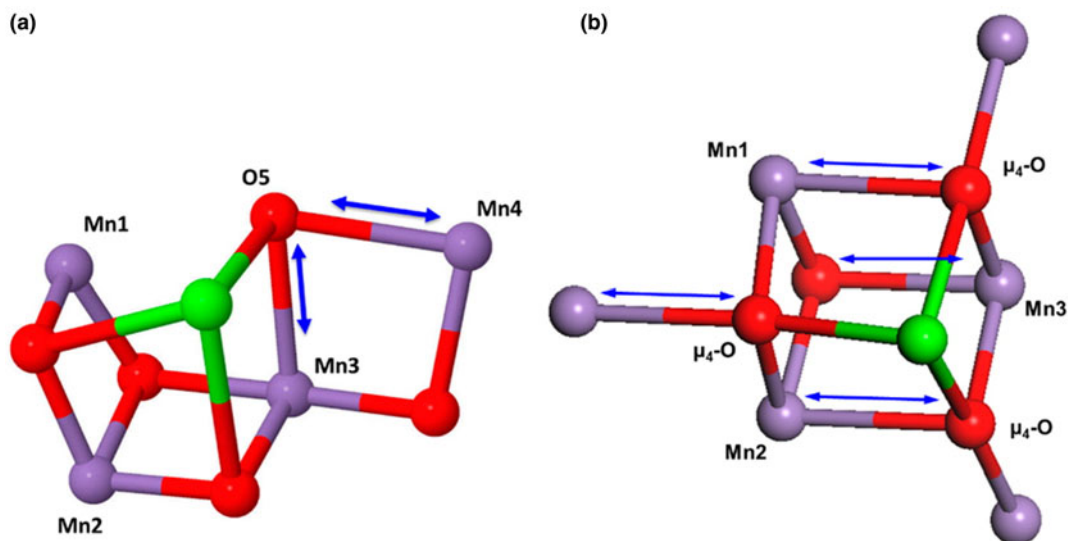


Fig. 2. Structure comparison of the active centres in (a) PSII and (b) Ca-birnessite. Reprinted with permission from Yang *et al.* (2015). Copyright 2015 American Chemical Society.

of photosynthesis, due to the similar fine structures of the oxygen-evolving centre (OEC) and Ca-birnessite (Fig. 2) (Russell, 2002; Sauer and Yachandra, 2002). In PSII, the photocatalytic oxygen production reaction occurs when Mn clusters, Mn_4CaO_5 , are converted into a birnessite-like structure (Hocking *et al.*, 2011). The Mn clusters have a cubic alkane structure, which is composed of highly distorted Mn_4Ca -oxo and overhanging Mn_4CaO_5 . During the process of photosynthesis (i.e. S-state cycle), the structure of Mn clusters and the oxidation state of Mn are changed (Fig. 3). Birnessite is a layered mineral with a repeated single-layer of MnO_2 . Each MnO_2 layer is composed of $[MnO_6]$ octahedra with shared edges, and the interlayer between MnO_2 layers contains alkaline cations and water molecules (Robinson *et al.*, 2013). The photocatalytic decomposition of water by birnessite (Fig. 4) is similar to the S-state cycle of PSII described above, in which the processes both consist of the first oxidation of Mn (III), the formation of O–O bonds and the final reduction of Mn(IV) (Yang *et al.*, 2015; Table 3).

There are two opinions on the evolution of the Mn_4CaO_5 cluster. The first is that the OEC evolved from Mn-bearing proteins, whereby the transfer of electrons by Mn-bearing catalase may be the intermediate step of aerobic photosynthesis (Blankenship and Hartman, 1998). However, there is no obvious similarity between the PSII core protein and Mn-bearing catalase, and there is no evidence that H_2O_2 was abundant in the Archean ocean. Olson (1970) proposed a hypothesis that Mn(III)–porphyrin cytochrome could replace Fe-bearing cytochromes in the evolution of OEC and pointed out a series of nitrogen-containing compounds such as NO and NO_2^- as transition electron donors of intermediate redox potential (Olson, 1970). However, from today's perspective of OEC, this may be incorrect because Mn is not bound in cytochrome but exists in Mn_4CaO_5 clusters, and whether the transition state of nitrogen compounds existed at that time is still questionable (Sauer and Yachandra, 2002).

The other viewpoint is that OEC is derived from the integration of Mn oxides, because OEC is similar to some layered Mn oxides (e.g. birnessite) in the short-range structure (Russell, 2002; Sauer and Yachandra, 2002; Russell *et al.*, 2008). However, there is no integration process of Mn oxides in the

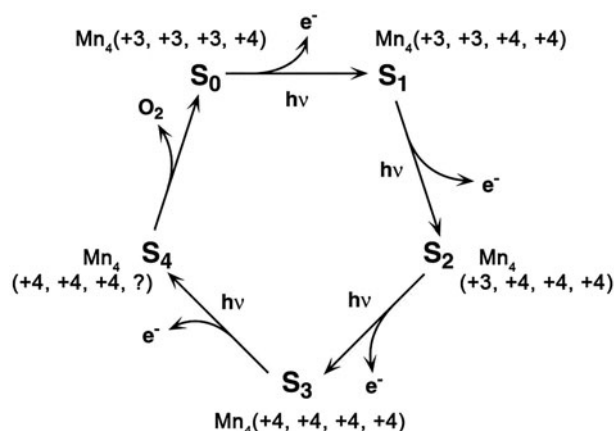


Fig. 3. The Kok cycle of S-state transitions in photosynthetic water oxidation (Reprinted with permission from Sauer and Yachandra, 2002, Copyright (2002) National Academy of Sciences).

formation of OEC (Tamura and Chenaie, 1987; Johnson *et al.*, 2013). If that occurred, the OEC-like function of natural Mn oxides would have made a pioneering contribution to atmospheric oxygen before the Great Oxidation Event of primitive Earth. Moreover, such a model for abiotic oxygen production has been probably working on Mars, where Mn oxides have always been abundant and exposed to the Sun (as described for the Earth above) (e.g. Lanza *et al.*, 2016).

Vast distribution of Mn oxides on modern Earth

Manganese oxides are widespread in modern natural settings especially in both oceanic and terrestrial environments (Post, 1999; McKeown and Post, 2001; Dorn, 2007; Nash *et al.*, 2007; Lu *et al.*, 2019a). They are the predominant components of Mn nodules that develop across the ocean floor and on the bottom of fresh-water lakes (Bauman, 1976; Jiang *et al.*, 2007). These Mn oxides are generally birnessite, todorokite and vernadite (Burns and Burns, 1977; Manceau *et al.*, 2014). The formation

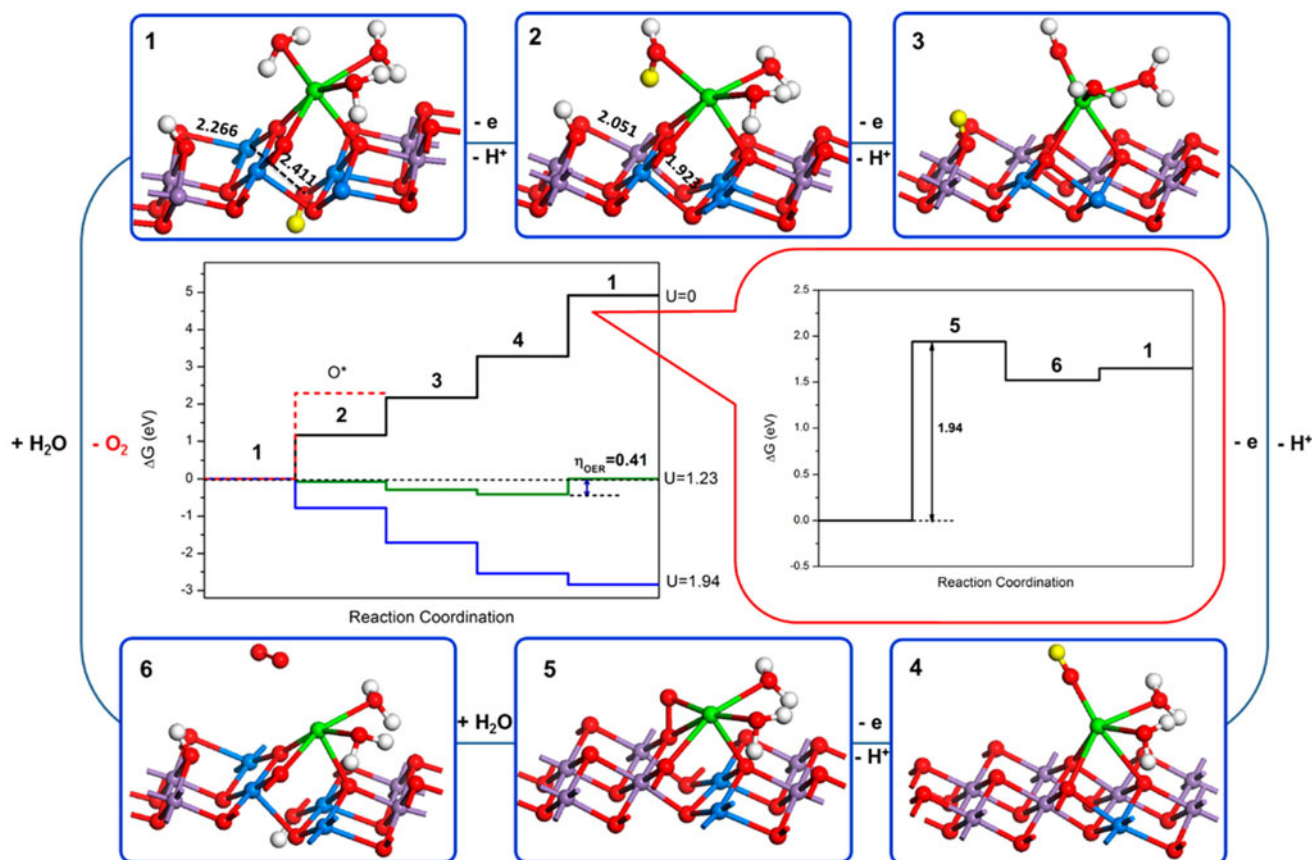


Fig. 4. Scheme of water oxidation on the surface of Ca-birnessite. The purple and blue atoms represent Mn (IV) and Mn (III), respectively. The yellow proton represents the proton to remove in the next step (Reprinted with permission from Yang *et al.* (2015). Copyright 2015 American Chemical Society).

Table 3. Comparison of photocatalytic decomposition of water by PSII oxygen production and birnessite.

Reaction	PSII	Birnessite
Mn (III) is gradually oxidised	S ₁ -S ₃	S ₁ -S ₄
O-O bond is formed	S ₄	S ₅
Mn (IV) is reduced, H ₂ O is oxidised and O ₂ is released	S ₄ -S ₀ -S ₁	S ₅ -S ₆ -S ₁

of Mn-enriched nodules is thought to arise from upward diffusion of Mn through the underlying reducing sediments and further accumulated by the catalytic oxidation of Mn(II) adsorbed on preliminarily formed fine-grained MnO₂ (Lei and Bostrom, 1995). In addition, some Mn-oxidising bacteria (such as *Pseudomonas putida* and *Bacillus* species) have been found in marine nodules, which are considered responsible for the biogenic origin of Mn oxides (Crerar and Barnes, 1974; Tebo *et al.*, 2004; Webb *et al.*, 2005; Villalobos *et al.*, 2006).

In terrestrial settings, Mn is the second most abundant heavy metal element in the Earth's crust, of which Mn(IV/III) are the most prevalent forms (Tebo *et al.*, 2004). In terrestrial weathering environments especially, the most representative Mn deposits are rock varnish, which attaches typically to the uppermost surface of rocks from arid to semiarid regions such as in the Gobi Desert (McKeown and Post, 2001; Nash *et al.*, 2007; Xu *et al.*, 2018). The Mn enrichment of rock varnish has been reported to be ~50–200 times of that in upper crust (Thiagarajan and Lee, 2004; Dorn, 2007; Goldsmith *et al.*, 2014; Xu *et al.*, 2019), and

the dominant Mn oxide phases are birnessite, todorokite and romanèchite (McKeown and Post, 2001; Garvie *et al.*, 2008; Xu *et al.*, 2018; Lu *et al.*, 2019a). Several formation mechanisms for rock varnish have been proposed. Thiagarajan and Lee (2004) and Goldsmith *et al.* (2014) proposed direct aqueous atmospheric deposition as one method, whereas Northup *et al.* (2010) suggested that biogenic Mn oxidation by fungi and bacteria will also induce Mn nucleation and precipitation. Recently, Xu *et al.* (2018, 2019) put forward a new theory that light-enhanced photocatalytic oxidation of Mn by semiconducting minerals such as Fe oxides co-present in rock varnish is responsible for its formation.

Widespread Mn coatings on the Earth's surface

The Mn (oxyhydr)oxide mineral coatings are found to overlay vast expanses of natural rock/soil surfaces in various natural environments (Lu *et al.*, 2019a). These Mn coatings are usually tens to hundreds of micrometres in thickness. In arid and semi-arid regions, they are typically dark brown in colour and well separated from the substrate rocks by a distinct interface. Manganese coatings in relatively humid areas, such as karst regions with limestone deposits, are dark-grey in colour and porous in structure. The soil coatings (i.e. soil cutans) are generally red to dark brown, wrapping around quartz, feldspar particles and clay mineral aggregates. Lu *et al.* (2019b) and Xu *et al.* (2019) discovered that the Mn coatings were generally developed on the upper rock surfaces that are exposed to abundant solar irradiation. The geographical distribution of Mn coatings exactly

coincides with intense solar irradiation regions around the Earth (Lu *et al.*, 2019a). All these lines of evidence suggest that sunlight has the greatest effect on the formation of Mn coatings on the Earth's surface. In laboratory studies, the photo-generated reactive oxygen species (such as $^1\text{O}_2$ and OH^\cdot) in rock varnish have been detected, providing direct evidence for the model proposed by Xu *et al.* (2019).

Birnessite is the primary Mn oxide found in Mn coatings, whereas tunnelled Mn oxides (such as todorokite, romanèchite and hollandite) possibly occur in desert Mn coatings or soil cutans, and Mn(II)-carbonate has been found in karst Mn coatings (McKeown and Post, 2001; Lu *et al.*, 2019a; Xu *et al.*, 2019). Moreover, the fine structural features of Mn coatings can vary in different environmental settings. According to our recent investigations by X-ray absorption spectroscopy, the average Mn oxidation state was as low as 3.21 in soil cutans, whereas it could reach up to 3.62 in desert Mn coatings (unpublished work). In karst Mn coatings, nanocrystalline vernadite was most common (Lu *et al.*, 2019a), which possessed random layer stacking and abundant vacant sites in its structure (Post, 1999; Villalobos *et al.*, 2003; Villalobos *et al.*, 2006; Sherman and Peacock, 2010). Among semiconducting minerals, birnessite in Mn coatings has been revealed to exhibit highly responsive and stable photon-to-electron conversion and is expected to actively participate in the inorganic and organic redox chemistry on the Earth's surface (Sherman, 2005; Ling *et al.*, 2017; Lu *et al.*, 2019a).

Electronic structure of Mn oxides

Theoretical calculations have been applied widely to analyse the electronic structure of birnessite (Kwon *et al.*, 2009; Lucht and Mendoza-Cortes, 2015; Peng *et al.*, 2017). According to these results, the valence band and conduction band of birnessite consist mainly of O(2p) and Mn(3d) orbitals, respectively, whose electronic structure can be interpreted by crystal field theory (Fig. 5). Due to the repulsion between O ions and the 3d orbitals of Mn in the $[\text{MnO}_6]$ octahedron, Mn 3d orbitals would be split into t_{2g} (e.g. d_{xy} , d_{yz} and d_{zx}) symmetry and e_g (e.g. $d_{x^2-y^2}$ and d_{z^2}) symmetry (Sherman, 2005; Kwon *et al.*, 2009). Considering that 3d electron configuration of Mn(IV) ions is $t_{2g}^3 e_g^0$, the valence band maximum (VBM) of birnessite is occupied by the t_{2g} triplet and its conduction band minimum (CBM) is dominated by the e_g doublet (Xu and Schoonen, 2000). Mn (or O) vacancies and introduced transition metal cations change the band structure of birnessite and are discussed in detail below.

Effect of Mn (or O) vacancies

Manganese (or O) vacancies in birnessite can affect the electronic structure and reduce the bandgap (Kwon *et al.*, 2008, 2009). For Mn vacancies, the surrounding O around the Mn vacancy usually associates with four H atoms to balance the charge. By calculating the energy, the structure is stable when four extra H atoms lie out of the **ab** plane in proximity to each other (Ruetschi, 1984; Kwon *et al.*, 2009). Attributed to the Mn 3d and O 2p orbitals around the Mn-vacancy site, the bandgap decreases due to some newly-introduced states emerging above its VBM. Further, when increasing the Mn vacancies from 3.3% to 12.5%, the bandgap of birnessite shows a reducing trend (Fig. 5). The bandgap of non-vacancy birnessite is indirect, whereas the bandgap of birnessite with Mn vacancy is direct at Γ (Fig. 6a,b). There is also a difference in the CBM and VBM partial charge of non-vacancy and Mn-vacancy birnessite (Fig. 6c,d).

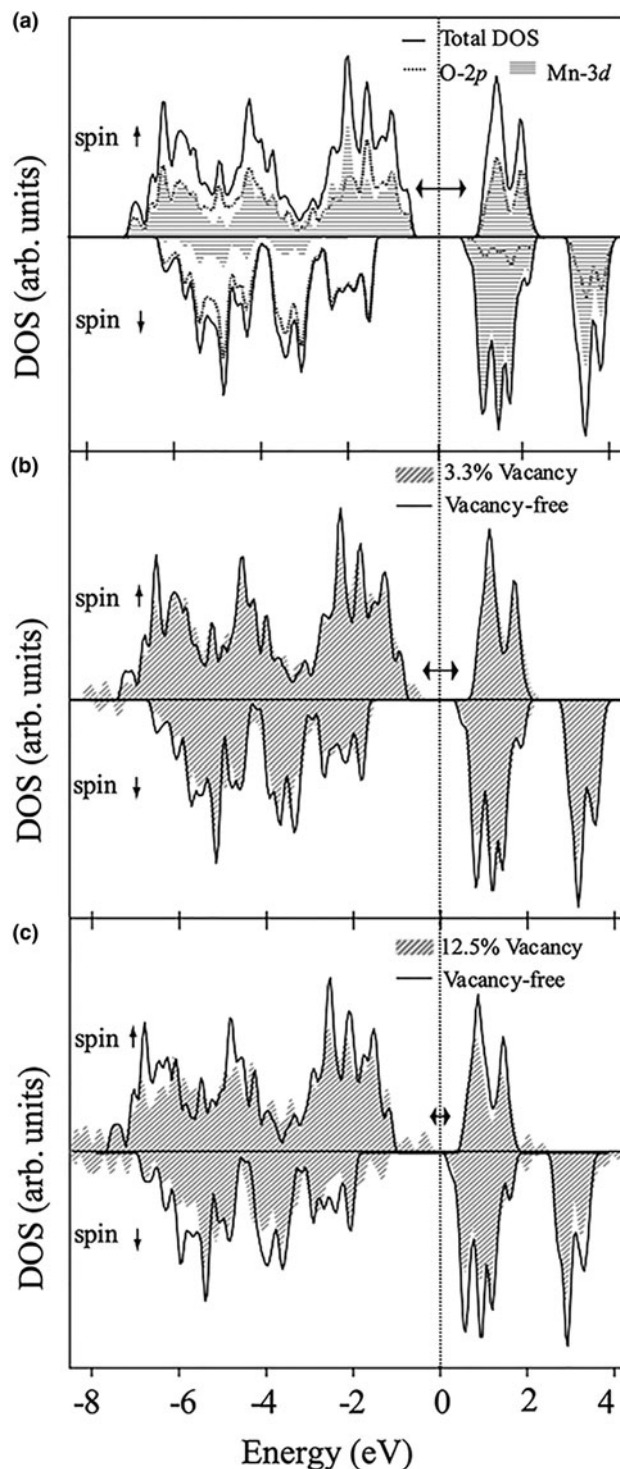


Fig. 5. The density of states (DOS) of (a) non-vacancy birnessite with its O 2p and Mn 3d contribution to the total DOS. Total DOS of birnessite with vacancies (filled areas) in a) $4 \times 4 \times 1$ supercell and c) $2 \times 2 \times 1$ supercell, with the corresponding total DOS of non-vacancy birnessite (from Kwon *et al.*, 2009).

In non-vacancy birnessite, most of the electron and hole states are overlapping, whereas they are well-separated in birnessite with Mn vacancies (Kwon *et al.*, 2009). The electronic transitions from valence band to conduction band upon illumination would leave holes at VBM and excited electrons at CBM. The separation between the

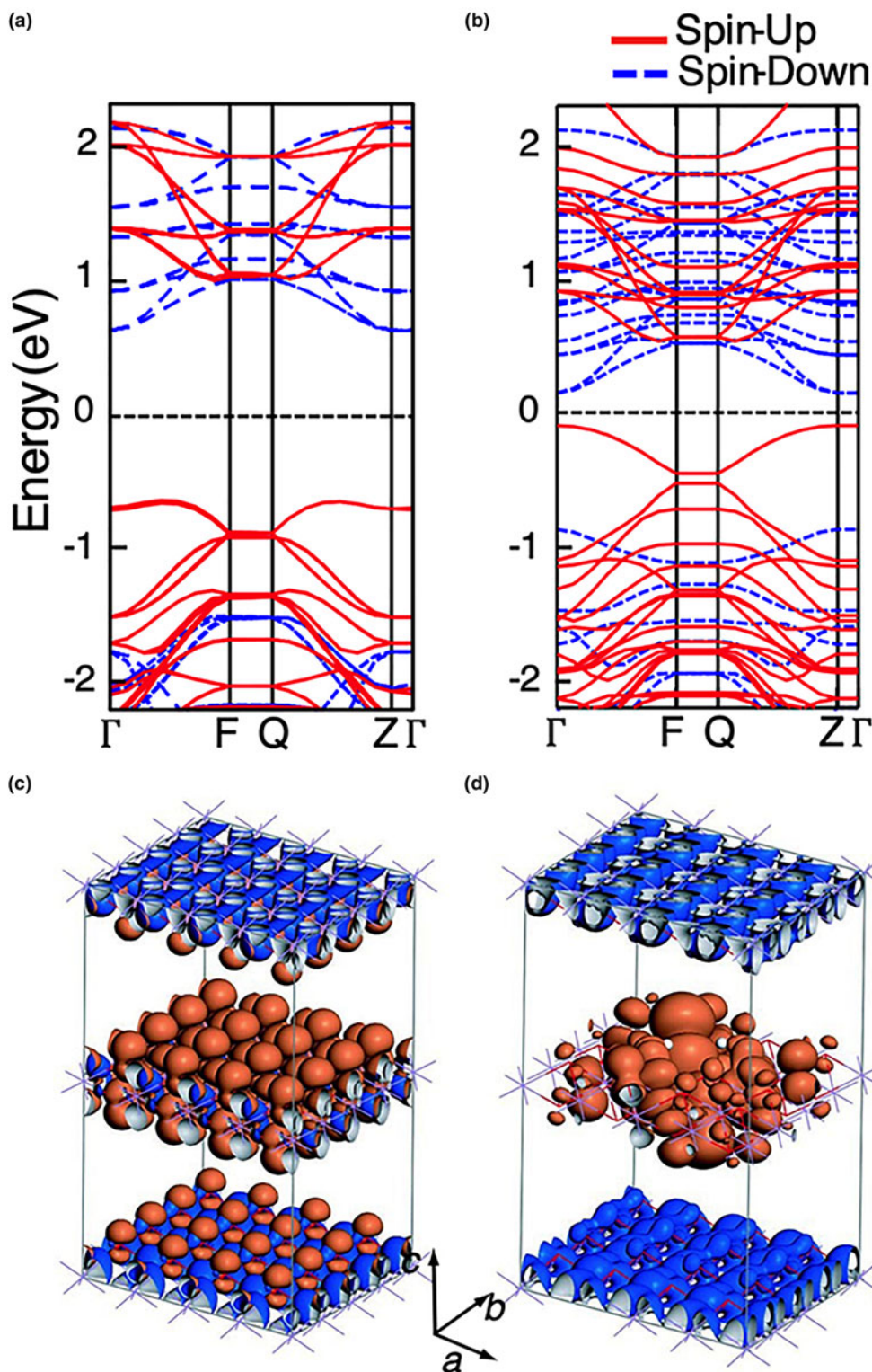


Fig. 6. MnO₂ band structure of (a) non-vacancy and (b) Mn-vacancy views of charge distributions of valence band maximum (VBM) hole states [orange or light grey] and conduction band minimum (CBM) electron states [blue or grey] in (c) non-vacancy and (d) Mn-vacancy (from Kwon *et al.*, 2008).

VBM and the CBM would promote photoinduced charge carriers efficiently.

Oxygen vacancies, another common defect in birnessite, has been proposed to have dual roles in the alteration of electronic structure. They can generate an extra electron in each [MnO₆]

octahedron and convert Mn(IV) ($t_{2g}^3 e_g^0$) into unstable high-spin Mn(III) ($t_{2g}^3 e_g^1$). To maintain a low-energy state in the strong Jahn–Teller effect, the extra electron must occupy another split Mn(III) d-orbital, i.e. e_g^1 (d_{z^2}) within the bandgap (Fig. 7) (Lucht and Mendoza-Cortes, 2015; Peng *et al.*, 2017). Such a

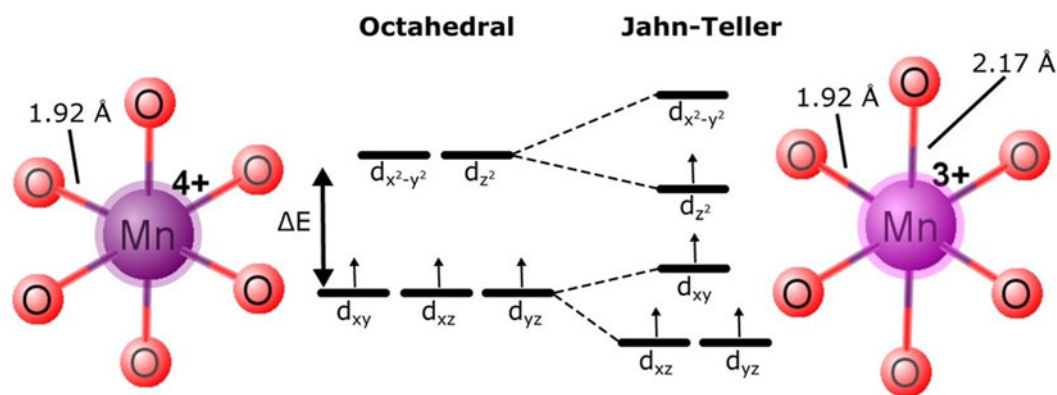


Fig. 7. For Mn^{3+} (right), the Jahn–Teller effect causes elongation of the Mn–O bond compared to Mn^{4+} (left). Because of the loss of degeneracy, the orbitals for the Mn^{3+} are offset to lower the energy of the partially filled orbitals. Reprinted with permission from Lucht and Mendoza-Cortes (2015). Copyright 2015 American Chemical Society.

configuration can remarkably decrease the bandgap of O-defected birnessite compared with the non-vacancy one. In contrast, O vacancies also commonly exist in other metal oxides and work as active sites in reactions (Wang *et al.*, 2017; Cao *et al.*, 2019). In Nature, multiple surfaces may be exposed and therefore perform different levels of photoactivity. Theoretical calculations have compared the function of O vacancies exposed on the (001) and (100) crystal face of birnessite. The formation energy of O vacancies is 1.45 eV for the (001) face and 1.43 eV for the (100) face, indicating the latter is more available than the former. The density of states (DOS) in Fig. 8 also shows O vacancies reduce the bandgap and the (100) crystal face exhibits half-metallicity characteristics with near-zero bandgap. These results suggest that O vacancies can effectively change the surface state, which is consistent with the experimental studies (Yang *et al.*, 2018).

Effect of metal cations

Cation exchange capacity is a significant property of layered minerals, which adsorb cations reversibly in order to compensate for the negative charge of layers (Mukhopadhyay, 2011). Transition metal cations are commonly observed in natural birnessite because of their similar crystal field environments with Mn ions. Generally, cations coordinate in two kinds of sites. One is cations incorporating into the birnessite sheet (INC), resulting in surrounding ions distorting and the second is cations forming triple-corner-sharing (TCS) in the interlayer of birnessite, resulting in $[\text{MnO}_6]$ layers with, either increased interlayer spacing, or expanded average bonding distances between Mn and O atoms. The electronic structure of birnessite will be changed in both cases. When Fe ions occupy a vacant Mn site, the bandgap of birnessite reduces because of Fe 3d orbitals mixing with Mn 3d and O 2p in VBM and CBM (Lucht and Mendoza-Cortes, 2015; Liu *et al.*, 2018a). For Cu cations, the influence of INC and TCS sites on the electronic structure has been discussed by Li *et al.* (2019a). The bandgap will shrink in both situations. Specifically, the bandgap of Cu ions in hexagonal birnessite reduces more in INC configuration compared with Cu ions in TCS, whereas for triclinic birnessite, the influence of Cu ions on the bandgap is greater in TCS than in INC.

Moreover, the electronic structure of transition metal cations will affect the coordination trend (i.e. in the TCS and INC model). For example, through simulating the INC and TCS

model of Co, Ni, Cu and Zn cations in birnessite, the energy difference between forming INC and TCS species is -214 , -23 , $+4$ and $+34$ kJ/mol, respectively. For INC models, with the increasing content of cations, it exerts greater stress on the surrounding ions by Jahn–Teller distortion through the interaction between the 3d orbitals of metal cations and ligands O. Qualitatively, with increasing electronic number of Co, Ni, Cu and Zn, the unoccupied 3d orbital reduces and thus decreases the Jahn–Teller distortion. In Zn ions, strong interaction would not happen due to fully occupied 3d orbitals, and the INC site for Zn is unstable in birnessite (Kwon *et al.*, 2013). The DOS of Zn in the INC site also shows the weak interaction because the 3d electronic is located mainly in a deep valence band without spin-exchange.

Photo-reactivity of natural semiconducting Mn oxides

Photocatalytic self-reduction of natural Mn oxides

In aquatic environments, the vertical profile of Mn in a multitude of oceanic and lacustrine water columns shows a gradual decrease in the concentration of aqueous Mn with depth (Klinkhammer and Bender, 1980; Landing and Bruland, 1987; Sunda and Huntsman, 1990; Davison, 1993; Statham *et al.*, 1998). Theoretically, aqueous Mn should be oxidised to Mn(III/IV) oxides by superoxide radicals generated by sunlight irradiation or organisms in the photic zone, resulting in lower concentrations. However, contrary to these thermodynamic estimates, aqueous Mn predominates in the photic zone (Sunda *et al.*, 1983; Tebo *et al.*, 2004; Morgan, 2005; Zhang *et al.*, 2018). This phenomenon is related to the photocatalytic self-reduction of natural Mn oxides, which can be caused either by a ligand-to-metal charge transfer process involving organics, or by the reduction of photoelectrons (Sunda *et al.*, 1983; Sunda and Huntsman, 1990, 1994). Narsito *et al.* (2008) showed that the charge transfer process involves three steps: (1) humic acid is adsorbed on the surface of MnO_2 to form an intermediate complex; (2) one delocalised π electron is excited and transferred; (3) one electron transfers from an oxygen centre to the manganese centre of an intermediate complex, causing the reductive dissociation of $\text{Mn(IV)} \rightarrow \text{Mn(II)}$ (Fig. 9a).

Manganese oxides have a suitable band gap of <3.1 eV and can absorb and convert photons to produce photoelectron-hole pairs under the excitation of visible light (Sherman, 2005). The photoelectrons/holes can change the valence states and existing forms of elements. It means the sunlight irradiation can induce

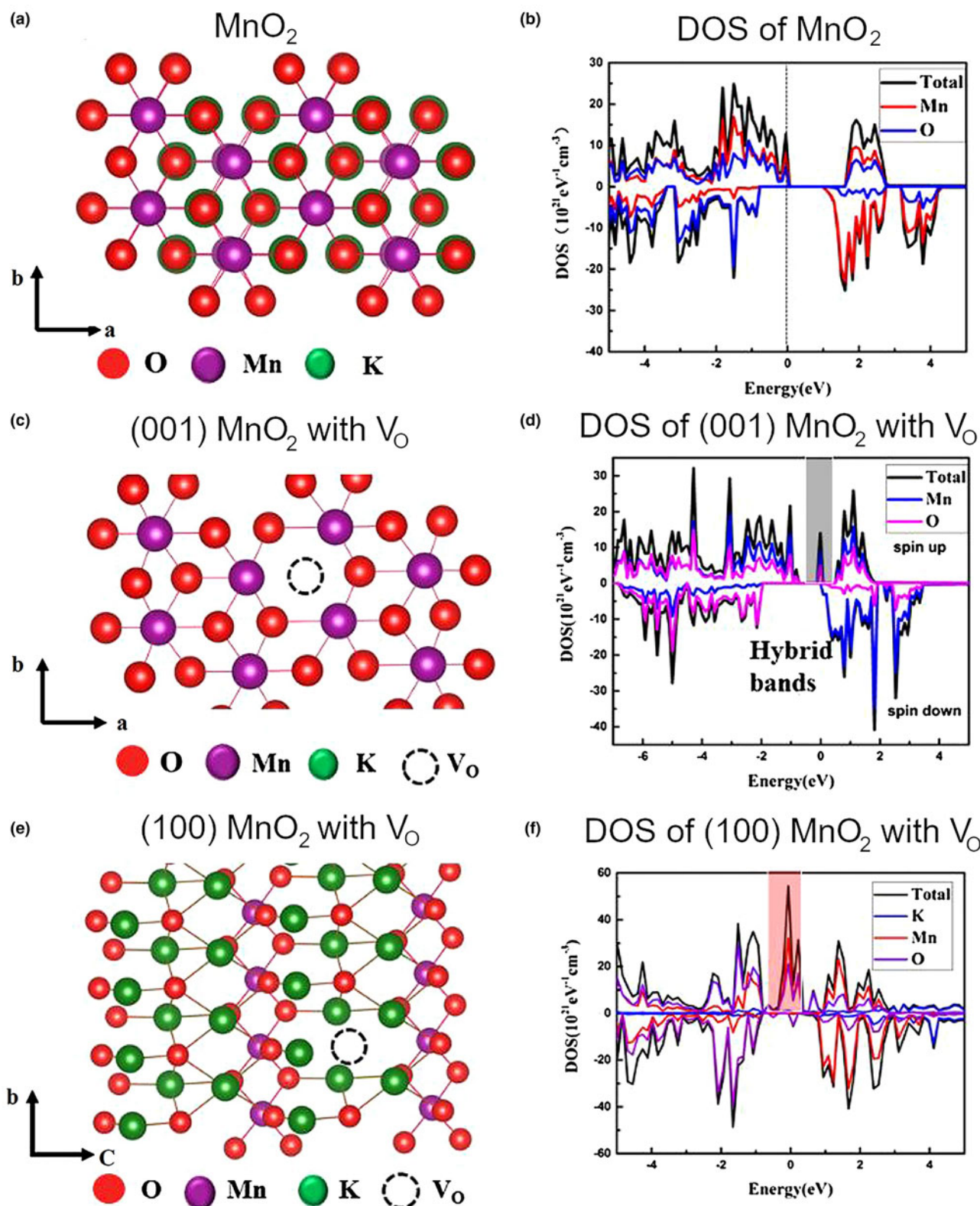


Fig. 8. (a,b) Top view of pure birnessite-type MnO₂ and corresponding DOS; (c,d) O vacancy configurations and corresponding DOS of (001) MnO₂; and (e,f) (100) MnO₂ (from Yang *et al.*, 2018).

photoelectrons in the Mn 3d orbitals in conduction bands and holes in O 2p orbitals in the valence band. If the electrochemical potential of the valence band is above one half-reaction then the

hole in the valence band could have oxidation potential (Sherman, 2005; Pinaud *et al.*, 2011). If the conduction-band potential is more negative than one half-reaction then the electron

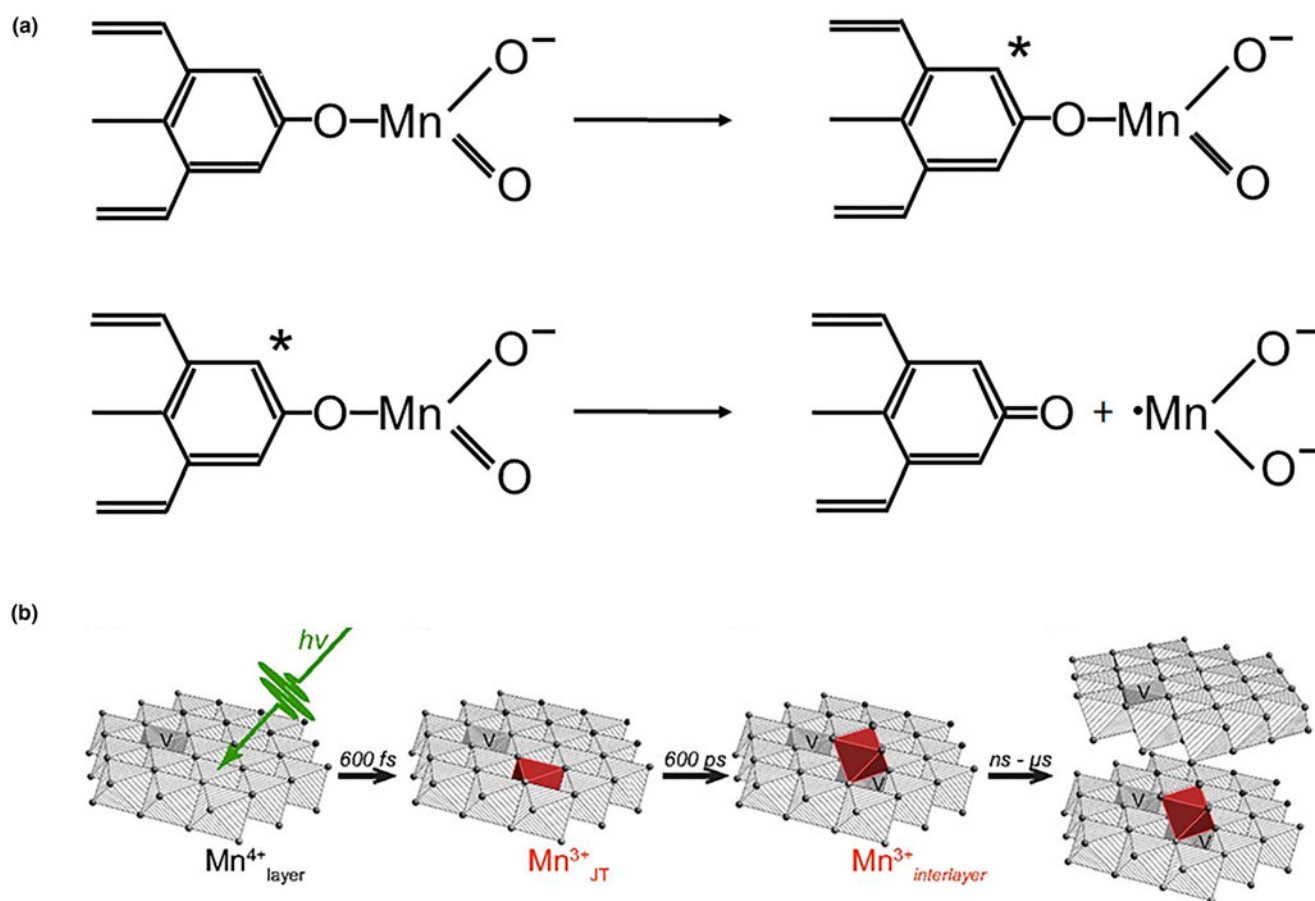


Fig. 9. (a) (Upper) Excitation of the humic acids aromatic system in the intermediate HA-MnO₂ complex through π-π* transition. (Lower) Reductive dissociation of excited intermediate of the HA-MnO₂ complex, producing water soluble Mn(II) of MnO₂²⁻ (from Narsito *et al.*, 2008). (b) Proposed model for the evolution of metal redox chemistry during δ-MnO₂ photoreduction (from Marafatto *et al.*, 2015).

excited into the conduction band would cause reduction. Sherman (2005) calculates that the conduction band for pyrolusite and birnessite are lower than the redox potential 1.23 V (SHE, Standard Hydrogen Electrode) of MnO₂/Mn(II); that is, they could theoretically adsorb sunlight to generate photoelectrons for self-photoreduction. Hence, a photoelectron could be excited to the conduction band to reduce Mn(IV) to Mn(III) under sunlight irradiation (Luther, 2005; Sakai *et al.*, 2005).

The valence band is occupied mainly by O 2p and e_g of Mn 3d orbitals. One electron in the O 2p orbital can transfer to the empty e_g orbital of Mn(IV) under sunlight irradiation to form intermediate Mn(III) (Luther, 2005; Sakai *et al.*, 2005). Mn(III) is in a tetragonally distorted rather than octahedral geometry, resulting in higher kinetic lability (ligand exchange) and reactivity (Marafatto *et al.*, 2015; Chan *et al.*, 2018). The e_g of Mn(III) therefore are prone to accept the photo-electron and thus the Mn(III) is further reduced to Mn(II) (Luther, 2005). Hence, the photocatalytic self-reduction of Mn oxides is a two-step one-electron transfer process. The conduction band states are localised Mn 3d orbitals that contribute to electron transfer, consequently, promoting the reduction of Mn(IV) to Mn(III). Marafatto *et al.* (2015) has proved the two-step one-electron transfer process by light-initiated time-resolved X-ray absorption spectroscopy (LITR-XAS). This involves the layered Mn(IV) oxide obtaining a photo-electron and being reduced to layered Mn(III) oxide; the Jahn-Teller distorted Mn(III) migrating into the interlayer; and then the interlayer

stacking increasing (Fig. 9b). In addition, the formation of valence band holes accompanying the photocatalytic self-reduction and the generation of Mn(III) can oxidise water or dissolved organic matter (Chan *et al.*, 2018). In addition, in the Raman spectra of the oxygen evolution reaction, Mn(III)-induced local strain on the oxide sublattice is observed, which further proves the one-electron transfer mechanism (Chan *et al.*, 2018).

Photocatalytic oxidation of water by Mn oxides

Although there are several Mn oxide minerals in natural environments, such as pyrolusite, todorokite, tithiophorite and hausmanite (Boppana and Jiao, 2011; Meng *et al.*, 2014; Huang *et al.*, 2019), only the birnessite local structure bears a striking similarity to the OEC in PSII (Fig. 10a,b) (Hocking *et al.*, 2011; Robinson *et al.*, 2013; Lucht and Mendoza-Cortes, 2015; Thenuwara *et al.*, 2015; Yang *et al.*, 2015). Consequently, the photo-oxidation activity of birnessite has drawn increasing attention, especially for water oxidation (Hocking *et al.*, 2011; Wiechen *et al.*, 2012; Thenuwara, *et al.*, 2015; McKendry *et al.*, 2018; Elmaci *et al.*, 2020).

The birnessite structure type is responsible for the high photocatalytic activity in the water oxidation process (Fig. 10). Hocking *et al.* (2011) found the tetranuclear Mn cluster [Mn₄O₄L₆] (L = diarylphosphinate), an efficient water-oxidation catalyst that converts to a birnessite-like structure during the water oxidation. This

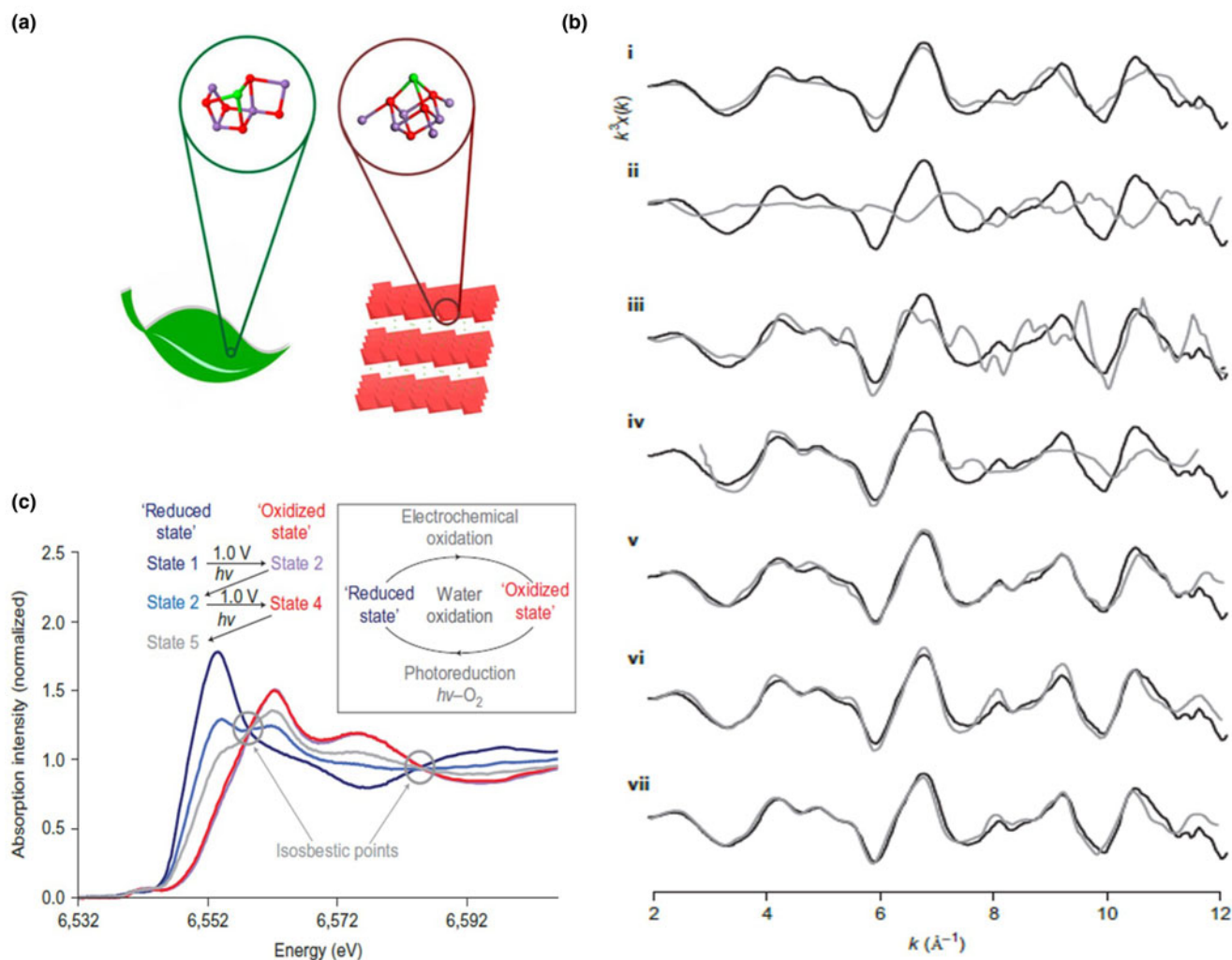


Fig. 10. (a) Structural comparison for Mn₄CaO₅ in natural vs. birnessite (Reprinted with permission from Yang *et al.* (2015). Copyright 2015 American Chemical Society). (b) Comparison of the extended X-ray absorption fine structure (EXAFS) spectra for several Mn oxides: i: [Mn₄O₄L₆](ClO₄); ii: [(bipy)₂Mn(O)₂Mn(bipy)₂](ClO₄); iii: Pyrolusite (1 × 1 tunnel); iv: Hollandite (2 × 2 tunnel); v: Todorokite (3 × 3 tunnel); vi: K-birnessite; vii: natural birnessite (disordered layer). (c) Comparison of X-ray absorption near edge structure (XANES) spectra during various states of catalytic cycling (from Hocking, *et al.*, 2011).

photoreactive process is similar to biological photosynthesis (Wiechen *et al.*, 2012) in thylakoids. Like Ca-cubane, birnessite also occurs in 5 states (S₀, S₁, S₂, S₃ and S₄) during photocatalytic water oxidation (Fig. 10c) (Hocking *et al.*, 2011). The valence states of the Mn ions are S₀ (+3, +3, +3, +4), S₁ (+3, +3, +4, +4), S₂ (+3, +4, +4, +4), S₃ (+4, +4, +4, +4) and S₄ (+4, +4, +4, ?) (Fig. 3) (Sauer and Yachandra, 2002; Cox *et al.*, 2013; Zhang *et al.*, 2015). The photocatalytic water oxidation by birnessite indicates the oxygen evolution on Earth is closely related to Mn oxides, which may have long been present through geological time prior to the emergence of biologic photosynthesis and Great Oxidation Event (Fig. 11).

Interestingly, on the Earth's surface, rare earth elements (REEs) are slightly enriched in mineral coatings compared with the underlying bedrock (Thiagarajan and Lee, 2004; Goldsmith *et al.*, 2014; Xu *et al.*, 2019). Particularly, the enrichment of cerium (Ce) in mineral coatings can reach 12 times, and Ce is concentrated in Mn-rich regions (Kalintsev *et al.*, 2021). The occurrence of Ce is either in the form of interlayer cations in birnessite, or as Ce(OH)_x nanoclusters adsorbed on corners of

birnessite layers. The ratio of Ce to Mn can reach 1:20 (wt.%) in samples (Lu *et al.*, 2019a,b). Similar Ce enrichment has been also reported in rock varnish of the arid desert over western America and the Middle East (Thiagarajan and Lee, 2004; Goldsmith *et al.*, 2014). Interlayer cations can also affect the photoactivity of Mn oxides (e.g. Wiechen *et al.*, 2012; Lucht and Mendoza-Cortes, 2015; Remsing *et al.*, 2015; Rong *et al.*, 2016). The different intercalated cations could tune the Jahn–Teller effect and adjust the hybridisation of electron orbits of birnessite, which in turn affects the electronic structure and band gap. By substituting the intercalated cations, it could tune the light capture ability and modify the intrinsic water-splitting catalytic property of birnessite. More specifically, Ce possesses a unique 4f electronic structure and properties of excellent oxygen adsorption and oxygen release, which are potentially advantageous for photocatalytic applications (Hernandez-Alonso *et al.*, 2004). The redox cycle of Ce(IV)–Ce(III) and oxygen vacancies in the structure enables it to have a strong oxygen storage capacity, which was beneficial to photocatalytic oxidation activity. For example, Ce_{1-x}Mn_xO₂ (x = 0, 0.1, 0.2, 0.3 and 1.0) samples

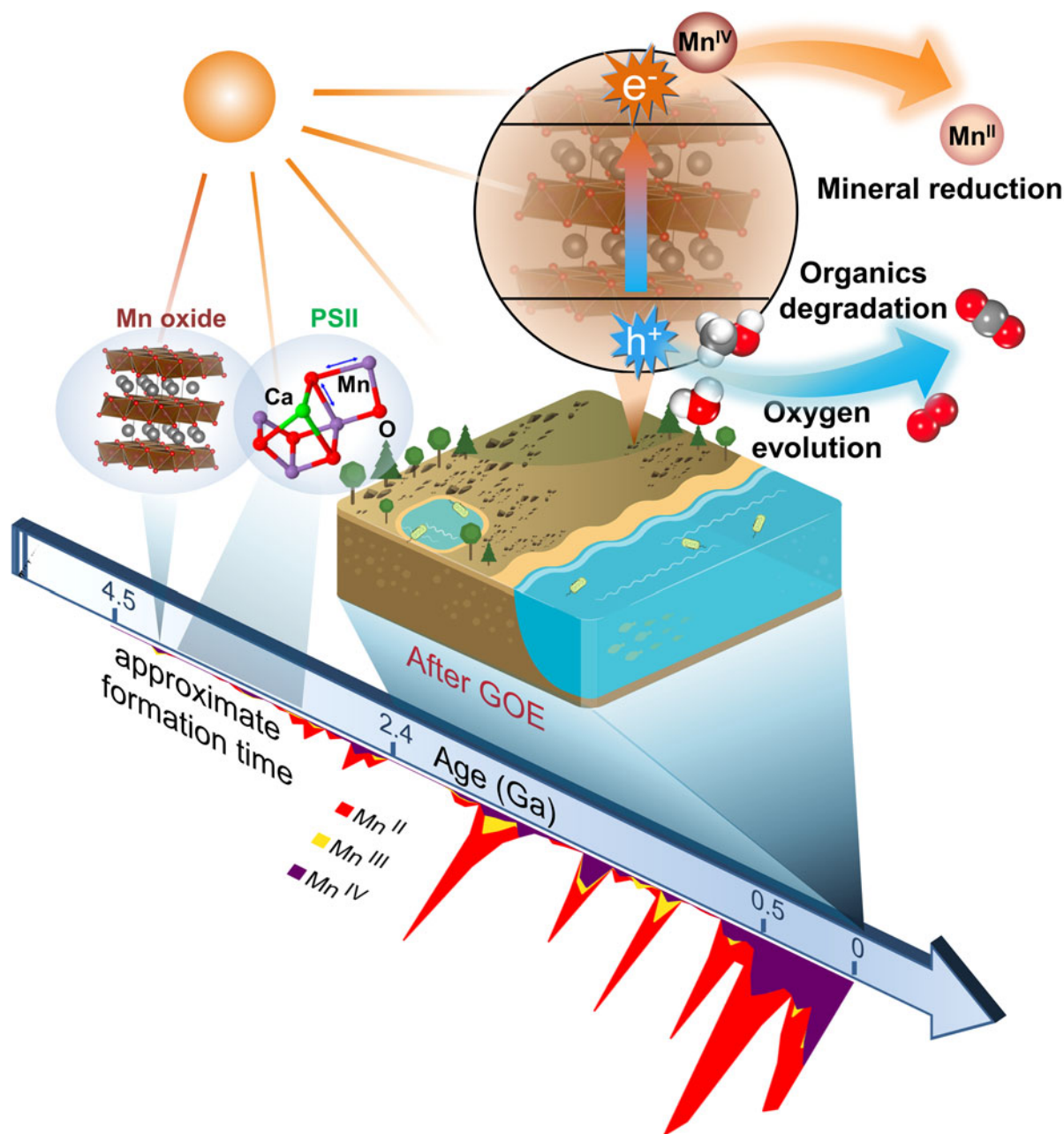


Fig. 11. Schematic model showing biogeochemical reactions dominated by photocatalytic Mn oxides on the sunlit Earth's surface in a long period of geological history. The evolution average oxidation state of Mn-bearing minerals (after Hazen *et al.*, 2019) is shown for indicating the formation time of Mn oxides.

have been used as photocatalysts for increasing the degradation efficiency of the textile diazo dye Naphthol Blue Black (Borker and Salker, 2006). More importantly, Gobi *et al.* (1993) reported that Mn Schiff base complexes in the presence of Ce(IV) could oxidise water. Hence, the enrichment and occurrence of Ce in mineral coatings can improve the understanding of the environmental functions of semiconducting minerals on the Earth's surface under sunlight.

It is noteworthy that the average abundances of Mn in the core, mantle and crust have low values, whereas Mn is extraordinarily concentrated in ultrathin layers of mineral coatings (Lu *et al.*, 2019a). We conclude that the solar light response and photocurrent production of widespread semiconducting mineral coatings

are capable of playing important roles in biogeochemical processes on the Earth's surface (Sunda *et al.*, 1983; Matsunaga *et al.*, 1995; Sherman, 2005; Lu *et al.*, 2019b), as shown schematically in Fig. 11. The photoelectrons from the conduction band of birnessite, similar to other semiconductors, can provide a driving force for the reduction of elements such as Mn, regenerate NADPH from NADP⁺ (Guo *et al.*, 2018), and provide a new form of energy for bacterial metabolisms (Lu *et al.*, 2012; Sakimoto *et al.*, 2016). The inexhaustible electron donors (e.g. water, organics and reduced ions) in Nature can complete those electron transport chains and bring about continuous redox chemistry, in which the semiconducting mineral coatings act as the vital bridge. Overall, the solar harvesting and photoelectric

converting properties of these coatings broaden the pathways for utilising solar energy from the well-known organic world to the mineral semiconductor world (Lu *et al.*, 2019b). As water, organic/inorganic matter and energy exchange on and penetrate through, these thin mineral coatings, it acts more like a functional ‘membrane’ covering the Earth’s surface; therefore, we can describe it as a ‘mineral membrane’.

Environmental functions of Mn oxides controlled by Mn redox cycling

Reductive dissolution of Mn oxides mediated by organic matter

In soil and sediment, Mn oxides are capable of reacting with surrounding organic matter such as citrate, oxalate, humic and fulvic acids (Stone, 1987; Wang and Stone, 2006a,b; Wang *et al.*, 2018; Flynn and Catalano, 2019). During redox reactions Mn(IV/III) will be reduced to low-valent Mn(III/II), some of which can detach from the structure and release off as soluble Mn(II) (Fig. 11). The mechanisms for the redox reactions between Mn oxides and organics are intrinsically attributed to the adsorption, complexation and reduction processes (Wang and Stone, 2006b). Adsorption refers to the formation of surface complexes, Mn(IV/III)–organic anions, which are essential to the reactions on the (hydr)oxide surfaces. Complexation induces the release of surface-located Mn(III) and the formation of Mn(III)-organic complexes in solution, which cause the ligand-assisted dissolution. Reduction processes involve the conversion of Mn(IV) and Mn(III) to dissolved Mn(II), i.e. reductive dissolution.

The reduction efficiency of Mn oxides is affected closely by pH condition. At more acidic pH, Mn reduction will proceed more completely and rapidly, giving rise to both the accumulation of structural Mn(III/II) and the massive dissolution of Mn oxides into Mn(II) (Stone and Morgan, 1984; Waite *et al.*, 1988; Wang and Stone, 2006b; Wang *et al.*, 2018; Flynn and Catalano, 2019). The H⁺-enhanced Mn reduction could be rationalised by the H⁺-consuming property of the birnessite–organics reaction (Wang *et al.*, 2018). Also, the protonation of the birnessite surface is beneficial for the surface adsorption of organic anions and thus facilitates further reactions (Stone and Morgan, 1984). In addition, Mn(II) desorption from edge sites into solutions will be promoted under acidic conditions (Wang and Stone, 2006a).

The dissolved Mn(II) and the structural Mn(III/II) could further modify the fine structures of Mn oxides, or even promote the inter-transformation among different mineral phases (Lefkowitz *et al.*, 2013; Hinkle *et al.*, 2016). For birnessite especially, the vacancy abundance, layer stacking, in-plane crystallinity within the phyllosilicate sheets and local coordination structure centring the Mn atoms will all be likely to alter (Wang *et al.*, 2018; Flynn and Catalano, 2019). Notably, these structural responses after the redox reaction with organics are also liable to be affected by pH conditions. In a weakly acid environment of pH 4–6, Mn(III/II) tends to migrate into the inter-layer space and adsorb in the layer above vacancies (Wang *et al.*, 2018; Flynn and Catalano, 2019), which will strengthen the layer stacking (Marafatto *et al.*, 2015; Flynn and Catalano, 2019); in contrast, some of the Mn(III) also appears to locate at the layer edge sites, which, together with the abundant presence of dissolved Mn(II) in acidic solutions, might help induce the re-ordering of layer sheets towards triclinic symmetry (Hinkle *et al.*, 2016; Flynn and Catalano, 2019). Under neutral to alkaline solutions, the generated Mn(III) is more likely to be incorporated into vacant sites and reside in the layer (Wang *et al.*, 2018); further,

with the effect of Mn(II), additional mineral phases may form, such as manganite, feitknechtite and hausmannite (Lefkowitz *et al.*, 2013; Wang *et al.*, 2018; Zhang *et al.*, 2018). In addition, Mn oxide minerals, such as birnessite, in the soil can be used as electron acceptors for microorganisms (such as the *Dietzia* species), accompanied with the oxidation of organic matter and fixation as carbonate minerals (e.g. rhodochrosite, Li *et al.*, 2019b). It thus can be summarised that the coupling effect of birnessite and microorganisms in the soil system under sunlight can convert atmospheric CO₂ into organics effectively and, further, into carbonate minerals assisting with carbon sequestration.

Oxidative formation of Mn oxides and heavy-metal sorption

Until recently, the formation mechanism of natural Mn oxides has been controversial, and mainly divided into biogenic and abiotic oxidation. Naturally occurring Mn-oxidising microorganisms (bacteria and fungi) are responsible for the biogenic catalytic oxidation of Mn(II) into Mn(III/IV) oxides (Tebo *et al.*, 2004; Webb *et al.*, 2005; Villalobos *et al.*, 2006). The key to the catalytic process should be attributed to the properly-modified pH and redox conditions of the local aqueous environment by microorganisms, or the release of metabolic products to oxidise Mn(II) chemically (Richardson *et al.*, 1988; Hullo *et al.*, 2001; Tebo *et al.*, 2004). By contrast, Mn(II) is stable as redox-neutral at pH values up to 8.5 and hence the abiotic homogeneous oxidation of Mn(II) is very slow and requires years for completion (Tebo *et al.*, 2005; Kim *et al.*, 2011). However, some researchers have observed the rapid photo-oxidative generation of Mn oxides by coexisting natural semiconducting iron (hydr)oxides, such as hematite and goethite (Madden and Hochella, 2005; Xu *et al.*, 2019). Also, the photo-stimulated production of reactive oxygen species in natural Mn coatings, like ¹O₂ and OH[•] with strong oxidising capability, can contribute to Mn oxide formation (Xu *et al.*, 2019).

During the oxidative formation of layered Mn oxides, i.e. birnessite, some heavy metal ions are likely to be adsorbed or incorporated into the structure, such as Cu²⁺, Pb²⁺, Zn²⁺ and Ni²⁺ (Sherman and Peacock, 2010; Zhu *et al.*, 2010; Wang *et al.*, 2012; Kwon *et al.*, 2013; Yin *et al.*, 2014; Qin *et al.*, 2017; Liu *et al.*, 2018b). As revealed in these studies, the sorption sites and binding structures of the metal ions can be varied: most commonly, they are inclined to migrate into interlayer space and bind above the vacancy, forming a triple-corner-sharing (TCS) complex; sometimes they tend to be incorporated into the layer vacancy as INC species; in addition, the metal ions can be adsorbed at layer edges to form multinuclear species by double corner-sharing or edge-sharing complexing (DCS or DES).

The sorption pathways of heavy metals largely affect their preferential binding sites. When the metal cations are simultaneously co-precipitated with birnessite, they will predominantly adsorb above the layer vacancies; when the metal cations are post-adsorbed to birnessite, they tend to be incorporated into the vacancies or bind at layer edges (Li *et al.*, 2019a). In contrast, the metal sorption mechanism is sensitively impacted by the fine structure of birnessite. A large interlayer space will allow the layer accommodation of metal cations to bind at vacancies as TCS and INC species (Zhu *et al.*, 2010; Wang *et al.*, 2012; Liu *et al.*, 2018b). These species will potentially induce the structural transformation towards tunnelled Mn oxides (Manceau *et al.*, 2014). In other cases when the birnessite is accumulated structurally with Mn(III), the metal ions will be repelled to the

edge sites (Liu *et al.*, 2018b; Li *et al.*, 2019a). The correspondingly formed DES and DCS complexes are structurally unsteady and readily released off from the layer, especially under extreme pH conditions (Qin *et al.*, 2017).

Concluding remarks

Manganese oxides distributed widely among various natural settings on Earth are diversified in mineral phase, crystal structure and Mn oxidation state. The most common Mn oxides on the Earth's surface occur in rock/soil surface Mn coatings, which are predominantly present as birnessite, which has a layered structure and can contain interlayer metal cations. Natural birnessite displays a marked photoelectric response to visible light and acts as a semiconducting material. The electronic structure is sensitive to the fine structure such as Mn/O vacancies and adsorbed metal ions. With excellent photocatalytic property, birnessite actively participates in the photoredox reactions on Earth, during which birnessite itself is reduced while organics and even water is oxidised. Notably, the water oxidation and oxygen-evolving centre in the biological photosynthesis system, Mn_4CaO_5 , features a birnessite-type structure. The oxidative formation of birnessite occurs mainly through bio-catalysis by microorganisms such as *Pseudomonas putida* and *Bacillus* species; in other cases, the photo-oxidation is mediated by coexisting semiconducting minerals or reactive oxygen species. Manganese oxides act as heavy-metal scavenger in the environment, while also acting to degrade organics as well as oxidise water. Together they are all involved in the biogeochemical cycle driven by Mn photocatalytic reduction and oxidation in Nature.

Acknowledgements. This work was supported by the National Natural Science Foundation of China (91851208, 91951114, 41820104003, 41872042), the National Key Research and Development Program of China (2019YFC1805901) and the DDE-IUGS Big Science Program.

References

- Bauman A.J. (1976) desert varnish and marine ferromanganese oxide nodules – congeneric phenomena. *Nature*, **259**, 387–388.
- Beukes N. J. and Gutzmer J. (1996) A volcanic–exhalative origin for the world's largest (Kalahari) manganese field. *Mineralium Deposita*, **31**, 242–245.
- Blankenship R.E. and Hartman H. (1998) The origin and evolution of oxygenic photosynthesis. *Trends in Biochemical Sciences (Amsterdam. Regular ed.)*, **23**, 94–97.
- Boppana V.B.R. and Jiao F. (2011) Nanostructured MnO_2 : an efficient and robust water oxidation catalyst. *Chemical Communications*, **47**, 8973–8975.
- Borker P. and Salker A.V. (2006) Photocatalytic degradation of textile azo dye over $\text{Ce}_{1-x}\text{Sn}_x\text{O}_2$ series. *Materials Science and Engineering B – Solid State Materials for Advanced Technology*, **133**, 55–60.
- Böttcher M.E. and Huckriede H. (1997) First occurrence and stable isotope composition of authigenic $\gamma\text{-MnS}$ in the central Gotland Deep (Baltic Sea). *Marine Geology*, **137**, 201–205.
- Burbidge E.M., Burbidge G.R., Fowler W.A. and Hoyle F. (1957) Synthesis of the Elements in Stars. *Review of Modern Physics*, **29**, 547–650.
- Burbidge G. (2008) B2FH, the cosmic microwave background and cosmology. *Publications of the Astronomical Society of Australia*, **25**, 30–35.
- Burns R.G. and Burns V.M. (1977) Marine manganese nodules. Pp. 185–248 in: *Marine Manganese Deposits* (Glasby GP, editor). Elsevier, Amsterdam.
- Cairncross B. and Beukes N.J. (2013) *The Kalahari Manganese Field-The Adventure Continues*. Random House Struik. Capetown, 394 pp.
- Cao R.R., Zhang P.Y., Liu Y. and Zheng X.M. (2019) Ammonium-treated birnessite-type MnO_2 to increase oxygen vacancies and surface acidity for stably decomposing ozone in humid condition. *Applied Surface Science*, **495**, 143607.
- Chan Z.M., Kitchaev D.A., Weker J.N., Schnedermann C., Lim K., Ceder G., Tumas W., Toney M.F. and Nocera D.G. (2018) Electrochemical trapping of metastable Mn^{3+} ions for activation of MnO_2 oxygen evolution catalysts. *Proceedings of the National Academy of Sciences of the United States of America*, **115**, E5261–E5268.
- Cox N., Pantazis D. A., Neese F. and Lubitz W. (2013) Biological water oxidation. *Accounts of Chemical Research*, **46**, 1588–1596.
- Crerar D.A. and Barnes H.L. (1974) Deposition of deep-sea manganese nodules. *Geochimica et Cosmochimica Acta*, **38**, 279–300.
- Davison W. (1993) Iron and manganese in lakes. *Earth-Science Reviews*, **34**, 119–163.
- Daye M., Klepac-Ceraj V., Pajusalu M., Rowland S., Farrell-Sherman A., Beukes N., Tamura N., Fournier G. and Bosak T. (2019) Light-driven anaerobic microbial oxidation of manganese. *Nature*, **576**, 311–314.
- Dorn R.I. (2007) Rock varnish. Pp. 246–297 in: *Geochemical Sediments and Landscapes* (D.J. Nash and S.J. McLaren, editors). Blackwell, Singapore.
- Elmaci G., Özgenç G., Kurz P. and Zumreoglu-Karan B. (2020) Enhanced water oxidation performances of birnessite and magnetic birnessite nanocomposites by transition metal ion doping. *Sustainable Energy & Fuels*, **4**, 3157–3166.
- Elmi C., Post J.E., Heaney P.J. and Ilton E.S. (2021) Effects of pH and Ca exchange on the structure and redox state of synthetic Na-birnessite. *American Mineralogist: Journal of Earth and Planetary Materials*, **106**, 15–27.
- Fan D., Liu T. and Ye J. (1992) The process of formation of manganese carbonate deposits hosted in black shale series. *Economic Geology*, **87**, 1419–1429.
- Flynn E.D. and Catalano J.G. (2019) Reductive transformations of layered manganese oxides by small organic acids and the fate of trace metals. *Geochimica et Cosmochimica Acta*, **250**, 149–172.
- Frei R., Gaucher C., Poulton S.W. and Canfield D.E. (2009) Fluctuations in Precambrian atmospheric oxygenation recorded by chromium isotopes. *Nature*, **461**, 250–253.
- Garvie L.A.J., Burt D.M. and Buseck P.R. (2008) Nanometer-scale complexity, growth, and diagenesis in desert varnish. *Geology*, **36**, 215–218.
- Gauthier-Lafaye F., Holliger P. and Blanc P.L. (1996) Natural fission reactors in the Franceville basin, Gabon: A review of the conditions and results of a “critical event” in a geologic system. *Geochimica et Cosmochimica Acta*, **60**, 4831–4852.
- Gobi K.V., Ramaraj R. and Kaneko M. (1993) Water oxidation catalyzed by heterogeneous Schiff-base manganese complex. *Journal of Molecular Catalysis*, **81**, L7–L11.
- Goldsmith Y., Stein M. and Enzel Y. (2014) From dust to varnish: Geochemical constraints on rock varnish formation in the Negev Desert, Israel. *Geochimica et Cosmochimica Acta*, **126**, 97–111.
- Guo J., Suastegui M., Sakimoto K.K., Moody V.M., Xiao G., Nocera D.G. and Joshi N.S. (2018) Light-driven fine chemical production in yeast biohybrids. *Science*, **362**, 813–816.
- Hazen R.M., Downs R.T., Eleish A., Fox P., Gagné O.C., Golden J.J., Grew E.S., Hummer D.R., Hystad G., Krivovichev S.V., Li C., Liu C., Ma X., Morrison S.M., Pan F., Pires A.J., Prabhu A., Ralph J., Runyon S.E. and Zhong H. (2019) Data-driven discovery in mineralogy: recent advances in data resources, analysis, and visualization. *Engineering (Beijing, China)*, **5**, 397–405.
- Hernandez-Alonso M.D., Hungria A.B., Martinez-Arias A., Fernandez-Garcia M., Coronado J.M., Conesa J.C. and Soria J. (2004) EPR study of the photo-assisted formation of radicals on CeO_2 nanoparticles employed for toluene photooxidation. *Applied Catalysis B – Environmental*, **50**, 167–175.
- Hinkle M.A.G., Flynn E.D. and Catalano J.G. (2016) Structural response of phyllo-manganates to wet aging and aqueous Mn(II) . *Geochimica et Cosmochimica Acta*, **192**, 220–234.
- Hocking R.K., Brimblecombe R., Chang L.-Y., Singh A., Cheah M.H., Glover C., Casey W.H. and Spiccia L. (2011) Water–oxidation catalysis by manganese in a geochemical-like cycle. *Nature Chemistry*, **3**, 461–466.
- Hoffman P.F. and Schrag D.P. (2010) The snowball Earth hypothesis: testing the limits of global change. *Terra Nova*, **14**, 129–155.
- Holland H.D. (2006) The oxygenation of the atmosphere and oceans. *Philosophical Transactions of the Royal Society, London B, Biological Sciences*, **361**, 903–915.
- Huang J., Dai Y., Singewald K., Liu C.-C., Saxena S. and Zhang H. (2019) Effects of MnO_2 of different structures on activation of peroxymonosulfate

- for bisphenol A degradation under acidic conditions. *Chemical Engineering Journal*, **370**, 906–915.
- Hullo M.F., Moszer I., Danchin A. and Martin-Verstraete I. (2001) CotA of *Bacillus subtilis* is a copper-dependent laccase. *Journal of Bacteriology*, **183**, 5426–5430.
- Jackson M.G. and Dasgupta R. (2008) Compositions of HIMU, EM1, and EM2 from global trends between radiogenic isotopes and major elements in ocean island basalts. *Earth and Planetary Science Letters*, **276**, 175–186.
- Jiang X.J., Lin X.H., Yao D., Zhai S.K. and Guo W.D. (2007) Geochemistry of lithium in marine ferromanganese oxide deposits. *Deep-Sea Research Part I – Oceanographic Research Papers*, **54**, 85–98.
- Johnson J.E., Webb S.M., Thomas K., Ono S., Kirschvink J.L. and Fischer W.W. (2013) Manganese-oxidizing photosynthesis before the rise of cyanobacteria. *Proceedings of the National Academy of Sciences of the United States of America*, **110**, 11238–11243.
- Johnson J.E., Webb S.M., Ma C. and Fischer W.W. (2016) Manganese mineralogy and diagenesis in the sedimentary rock record. *Geochimica et Cosmochimica Acta*, **173**, 210–231.
- Kalintsev A., Brugger J., Etschmann B. and Ram R. (2021) An in situ, micro-scale investigation of inorganically and organically driven rare-earth remobilisation during weathering. *Mineralogical Magazine*, **85**, <https://doi.org/10.1180/mgm.2021.4>
- Kasting J.F., Egger D.H. and Raeburn S.P. (1993) Mantle redox evolution and the oxidation state of the Archean atmosphere. *Journal of Geology*, **101**, 245–257.
- Kaufman A.J., Johnston D.T., Farquhar J., Masterson A.L., Lyons T.W., Bates S., Anbar A.D., Arnold G.L., Garvin J. and Buick R. (2007) Late Archean biospheric oxygenation and atmospheric evolution. *Science*, **317**, 1900–1903.
- Kendall B., Reinhard C.T., Lyons T.W., Kaufman A.J., Poulton S.W. and Anbar A.D. (2010) Pervasive oxygenation along late Archaean ocean margins. *Nature Geoscience*, **3**, 647–652.
- Kim S.S., Bargar J.R., Nealson K.H., Flood B.E., Kirschvink J.L., Raub T.D., Tebo B.M. and Villalobos M. (2011) Searching for biosignatures using electron paramagnetic resonance (EPR) analysis of manganese oxides. *Astrobiology*, **11**, 775–786.
- Klinkhammer G.P. and Bender M.L. (1980) The distribution of manganese in the Pacific Ocean. *Earth and Planetary Science Letters*, **46**, 361–384.
- Koschinsky A. and Heine J.R. (2017) Marine ferromanganese encrustations: archives of changing oceans. *Elements*, **13**, 177–182.
- Krinsley D., Dorn R.I. and DiGregorio B. (2009) Astrobiological implications of rock varnish in Tibet. *Astrobiology*, **9**, 551–562.
- Kwon K.D., Refson K. and Sposito G. (2008) Defect-induced photoconductivity in layered manganese oxides: a density functional theory study. *Physical Review Letters*, **100**, 146601.
- Kwon K.D., Refson K. and Sposito G. (2009) On the role of Mn(IV) vacancies in the photoreductive dissolution of hexagonal birnessite. *Geochimica et Cosmochimica Acta*, **73**, 4142–4150.
- Kwon K.D., Refson K. and Sposito G. (2013) Understanding the trends in transition metal sorption by vacancy sites in birnessite. *Geochimica et Cosmochimica Acta*, **101**, 222–232.
- Lalonde S. V. and Konhauser K. O. (2015) Benthic perspective on Earth's oldest evidence for oxygenic photosynthesis. *Proceedings of the National Academy of Sciences of the United States of America*, **112**, 995–1000.
- Landing W.M. and Bruland K.W. (1987) The contrasting biogeochemistry of iron and manganese in the Pacific ocean. *Geochimica et Cosmochimica Acta*, **51**, 29–43.
- Lanza N.L., Wiens R.C., Arvidson R.E., Clark B.C., Fischer W.W., Gellert R., Grotzinger J.P., Hurowitz J.A., McLennan S.M., Morris R.V., Rice M.S., Bell J.F., Berger J.A., Blaney D.L., Bridges N.T., Calef F., Campbell J.L., Clegg S.M., Cousin A., Edgett K.S., Fabre C., Fisk M.R., Forni O., Frydenvang J., Hardy K.R., Hardgrove C., Johnson J.R., Lasue J., Le Mouélic S., Malin M.C., Mangold N., Martin-Torres J., Maurice S., McBride M.J., Ming D.W., Newsom H.E., Ollila A.M., Sautter V., Schröder S., Thompson L.M., Treiman A.H., VanBommel S., Vaniman D.T., Zorzano M.P. and Los Alamos National Lab, L.A.N.M. (2016) Oxidation of manganese in an ancient aquifer, Kimberley formation, Gale crater, Mars. *Geophysical Research Letters*, **43**, 7398–7407.
- Lefkowitz J.P., Rouff A.A. and Elzinga E.J. (2013) Influence of pH on the reductive transformation of birnessite by aqueous Mn(II). *Environmental Science & Technology*, **47**, 10364–10371.
- Lei G.B. and Bostrom K. (1995) Mineralogical control on transition-metal distributions in marine manganese nodules. *Marine Geology*, **123**, 253–261.
- Li Y., Liu F.F., Xu X.M., Liu Y.W., Li Y.Z., Ding H.R., Chen N., Yin H., Lin H., Wang C.Q. and Lu A.H. (2019a) Influence of heavy metal sorption pathway on the structure of biogenic birnessite: Insight from the band structure and photostability. *Geochimica et Cosmochimica Acta*, **256**, 116–134.
- Li Y., Wang X., Li Y., Duan J., Jia H., Ding H., Lu A., Wang C., Nie Y. and Wu X. (2019b) Coupled anaerobic and aerobic microbial processes for Mn-carbonate precipitation: A realistic model of inorganic carbon pool formation. *Geochimica et Cosmochimica Acta*, **256**, 49–65.
- Ling F.T., Post J.E., Heaney P.J., Kubicki J.D. and Santelli C.M. (2017) Fourier-transform infrared spectroscopy (FTIR) analysis of triclinic and hexagonal birnessites. *Spectrochimica Acta – Part A: Molecular and Biomolecular Spectroscopy*, **178**, 32–46.
- Liu H., Gu W.L., Luo B.C., Fan P., Liao L.B., Tian E.K., Niu Y.Q., Fu J.Z., Wang Z., Wu Y.Y., Lv G.C. and Mei L.F. (2018a) Influence of Fe doping on the crystal structure, electronic structure and supercapacitance performance of birnessite [(Na,K)_x(Mn⁴⁺,Mn³⁺)₂O₄·1.5H₂O] with high areal mass loading. *Electrochimica Acta*, **291**, 31–40.
- Liu Y.W., Li Y., Chen N., Ding H.R., Zhang H.Q., Liu F.F., Yin H., Chu S.Q., Wang C.Q. and Lu A.H. (2018b) Cu(II) sorption by biogenic birnessite produced by *Pseudomonas putida* strain MnB1: structural differences from abiotic birnessite and its environmental implications. *CrystEngComm*, **20**, 1361–1374.
- Liu W., Hao J., Elzinga E.J., Piotrowiak P., Nanda V., Yee N. and Falkowski P.G. (2020) Anoxic photogeochemical oxidation of manganese carbonate yields manganese oxide. *Proceedings of the National Academy Science of the United States of America*, **117**, 22698–22704.
- Lu A., Li Y., Jin S., Wang X., Wu X.L., Zeng C., Li Y. and Dong H. (2012) Growth of non-phototrophic microorganisms using solar energy through mineral photocatalysis. *Nature Communications*, **3**, 1–8.
- Lu A., Li Y., Ding H., Xu X., Li Y., Ren G., Liang J., Liu Y., Hong H., Chen N., Chu S., Liu F., Li Y., Wang H., Ding C., Wang C., Lai Y., Liu J., Dick J., Liu K. and Hochella M.F., Jr. (2019a) Photoelectric conversion on Earth's surface via widespread Fe- and Mn-mineral coatings. *Proceedings of the National Academy Science of the United States of America*, **116**, 9741–9746.
- Lu A., Li Y., Ding H. and Wang C. (2019b) “Mineral membrane” of the surface: “New sphere” of the Earth. *Acta Petrologica Sinica*, **35**, 119–128.
- Lucht K.P. and Mendoza-Cortes J.L. (2015) Birnessite: a layered manganese oxide to capture sunlight for water-splitting catalysis. *Journal of Physical Chemistry C*, **119**, 22838–22846.
- Luther G.W. (2005) Manganese(II) oxidation and Mn(IV) reduction in the environment – Two one-electron transfer steps versus a single two-electron step. *Geomicrobiology Journal*, **22**, 195–203.
- Lyons T., Reinhard C. and Planavsky N. (2014) The rise of oxygen in Earth's early ocean and atmosphere. *Nature*, **506**, 307–315.
- Lyons T.W., Diamond C.W. and Konhauser K.O. (2020) Shedding light on manganese cycling in the early oceans. *Proceedings of the National Academy of Sciences of the United States of America*, **117**, 25960–25962.
- Madden A.S. and Hochella M.F. (2005) A test of geochemical reactivity as a function of mineral size: Manganese oxidation promoted by hematite nanoparticles. *Geochimica et Cosmochimica Acta*, **69**, 389–398.
- Manceau A., Lanson M. and Takahashi Y. (2014) Mineralogy and crystal chemistry of Mn, Fe, Co, Ni, and Cu in a deep-sea Pacific polymetallic nodule. *American Mineralogist*, **99**, 2068–2083.
- Marafatto F.F., Strader M.L., Gonzalez-Holguera J., Schwartzberg A., Gilbert B. and Pena J. (2015) Rate and mechanism of the photoreduction of birnessite (MnO₂) nanosheets. *Proceedings of the National Academy of Sciences of the United States of America*, **112**, 4600–4605.
- Martino I. (1986) The minerals industry of Mexico. Pp. 553–573 in: *Area Reports: International Minerals Yearbook 1984*, Vol. 3, US Bureau of Mines.
- Matsumoto R. (1992) Diagenetic dolomite, calcite, rhodochrosite, magnesite, and lansfordite from Site 799, Japan Sea – Implications for depositional environments and the diagenesis of organic-rich sediments. Pp. 75–98 in: *Proceedings of the Ocean Drilling Program, Scientific Results* (Pisciotto

- K.A., Ingle J.C. Jr., von Breyman M.T., Barron J., et al., editors). Vol. 127/128, Pt. 1. Ocean Drilling Program, College Station, Texas, USA, <https://doi.org/10.2973/odp.proc.sr.127128-1.119.1992>
- Matsunaga K., Ohya T., Kuma K., Kudo I. and Suzuki Y. (1995) Photoreduction of manganese-dioxide in seawater by organic-substances under ultraviolet or sunlight. *Water Research*, **29**, 757–759.
- Maynard J.B. (2010) The chemistry of manganese ores through time: a signal of increasing diversity of earth-surface environments. *Economic Geology*, **105**, 535–552.
- McKeown D.A. and Post J.E. (2001) Characterization of manganese oxide mineralogy in rock varnish and dendrites using X-ray absorption spectroscopy. *American Mineralogist*, **86**, 701–713.
- McKendry I. G., Thenuwara A. C., Shumlas S. L., Peng H., Aulin Y. V., Chinnam P. R., Borguet E., Strongin D. R. and Zdilla M. J. (2018). Systematic doping of cobalt into layered manganese oxide sheets substantially enhances water oxidation catalysis. *Inorganic Chemistry*, **57**, 557–564.
- Meng B., Zhao Z., Chen Y., Wang X., Li Y. and Qiu J. (2014) Low-temperature synthesis of Mn-based mixed metal oxides with novel fluffy structures as efficient catalysts for selective reduction of nitrogen oxides by ammonia. *Chemical Communications*, **50**, 12396–12399.
- Morgan J.J. (2005) Kinetics of reaction between O₂ and Mn(II) species in aqueous solutions. *Geochimica et Cosmochimica Acta*, **69**, 35–48.
- Mukhopadhyay S. (2011) Clays: Colloidal properties in nanomedicine. *Nature Proceedings*, <https://doi.org/10.1038/npre.2011.5807.1>
- Narsito N., Santosa S.J. and Lastuti S. (2008) Photo-reduction kinetics of MnO₂ in aquatic environments containing humic acids. *Indonesian Journal of Chemistry*, **8**, 37–41.
- Nash D.J. and McLaren S.J. (2007) Introduction: geochemical sediments in landscapes. Pp. 1–9 in: *Geochemical Sediments and Landscapes* (D.J. Nash and S.J. McLaren, editors). Blackwell Publishing, UK.
- Nealson K.H. (2015) Ex-phot: a new take on primitive utilization of solar energy. *Environmental Microbiology Reports*, **7**, 33–35.
- Northup D.E., Snider J.R., Spilde M.N., Porter M.L., Van De Kamp J.L., Boston P.J., Nyberg A.M. and Bargar J.R. (2010) Diversity of rock varnish bacterial communities from Black Canyon, New Mexico. *Journal of Geophysical Research – Biogeosciences*, **115**, <https://doi.org/10.1029/2009JG001107>
- Olson J.M. (1970) The evolution of photosynthesis. *Science*, **168**, 438–446.
- Owen and Bricker. (1965) Some stability relations in the system Mn–O₂–H₂O at 25° and one atmosphere total pressure. *American Mineralogist*, **50**, 1296–1354.
- Peng H., McKendry I.G., Ding R., Thenuwara A.C., Kang Q., Shumlas S.L., Strongin D.R., Zdilla M.J. and Perdeu J.P. (2017) Redox properties of birnessite from a defect perspective. *Proceedings of the National Academy of Sciences of the United States of America*, **114**, 9523–9528.
- Piacentini T., Vasconcelos P.M. and Farley K.A. (2013) ⁴⁰Ar/³⁹Ar constraints on the age and thermal history of the Urucum Neoproterozoic banded iron-formation, Brazil. *Precambrian Research*, **228**, 48–62.
- Pinaud B.A., Chen Z., Abram D.N. and Jaramillo T.F. (2011) Thin films of sodium birnessite-type MnO₂: optical properties, electronic band structure, and solar photoelectrochemistry. *The Journal of Physical Chemistry C*, **115**, 11830–11838.
- Post J.E. (1999) Manganese oxide minerals: crystal structures and economic and environmental significance. *Proceedings of the National Academy of Sciences of the United States of America*, **96**, 3447–3454.
- Qin Z.J., Xiang Q.J., Liu F., Xiong J., Koopal L.K., Zheng L.R., Ginder-Vogel M., Wang M.X., Feng X.H., Tan W.F. and Yin H. (2017) Local structure of Cu²⁺ in Cu-doped hexagonal turbostratic birnessite and Cu²⁺ stability under acid treatment. *Chemical Geology*, **466**, 512–523.
- Remington R.C., McKendry I.G., Strongin D.R., Kein M.L. and Zdilla M.J. (2015) Frustrated solvation structures can enhance electron transfer rates. *Journal of Physical Chemistry Letters*, **6**, 4804–4808.
- Reinhard C.T., Raiswell R., Scott C., Anbar A.D. and Lyons T.W. (2009) A late Archean sulfidic sea stimulated by early oxidative weathering of the continents. *Science*, **326**, 713–716.
- Richardson L.L., Aguilar C. and Nealson K.H. (1988) Manganese oxidation in pH and O₂ microenvironments produced by phytoplankton. *Limnology and Oceanography*, **33**, 352–363.
- Robinson D.M., Go Y.B., Mui M., Gardner G., Zhang Z., Mastrogianni D., Garfunkel E., Li J., Greenblatt M. and Dismukes G.C. (2013) Photochemical water oxidation by crystalline polymorphs of manganese oxides: structural requirements for catalysis. *Journal of the American Chemical Society*, **135**, 3494–3501.
- Rong F., Zhao J., Chen Z., Xu Y., Zhao Y., Yang Q. and Li C. (2016) Highly active water oxidation on nanostructured biomimetic calcium manganese oxide catalysts. *Journal of Materials Chemistry A*, **4**, 6585–6594.
- Roy S. (1997) Genetic diversity of manganese deposition in the terrestrial geological record. Pp. 5–27 in: *Manganese Mineralization: Geochemistry and Mineralogy of Terrestrial and Marine Deposits* (K. Nicholson, J.R. Hein, B. Bühn and S. Dasgupta, editors). Geological Society London Special Publications, **119**.
- Roy S. (2006) Sedimentary manganese metallogenesis in response to the evolution of the Earth system. *Earth Science Reviews*, **77**, 273–305.
- Ruetschi P. (1984) Cation–vacancy model for MnO₂. *Journal of the Electrochemical Society*, **131**, 2737–2744.
- Russell M.J. (2002) From geochemistry to biochemistry: Chemiosmotic coupling and transition element clusters in the onset of life and photosynthesis. *The Geochemical News*, **113**, 6–12.
- Russell M.J., Allen J.F. and James M.W.E. (2008) Inorganic complexes enabled the onset of life and oxygenic photosynthesis. Photosynthesis. Pp. 1187–1192 in: *Energy from the Sun* (J.F. Allen, E. Gantt, J.H. Golbeck and B. Osmond, editor). Springer Netherlands.
- Sakai N., Ebina Y., Takada K. and Sasaki T. (2005) Photocurrent generation from semiconducting manganese oxide nanosheets in response to visible light. *Journal of Physical Chemistry B*, **109**, 9651–9655.
- Sakimoto K.K., Wong A.B. and Yang P. (2016) Self-photosensitization of non-photosynthetic bacteria for solar-to-chemical production. *Science*, **351**, 74–77.
- Sauer K. and Yachandra V.K. (2002) A possible evolutionary origin for the Mn₄ cluster of the photosynthetic water oxidation complex from natural MnO₂ precipitates in the early ocean. *Proceedings of the National Academy of Sciences of the United States of America*, **99**, 8631–8636.
- Schindler M. and Dorn R.I. (2017) Coatings on rocks and minerals: The interface between the lithosphere and the biosphere, hydrosphere, and atmosphere. *Elements*, **13**, 155–158.
- Sherman D.M. (2005) Electronic structures of iron(III) and manganese(IV) (hydr)oxide minerals: Thermodynamics of photochemical reductive dissolution in aquatic environments. *Geochimica et Cosmochimica Acta*, **69**, 3249–3255.
- Sherman D.M. and Peacock C.L. (2010) Surface complexation of Cu on birnessite (δ-MnO₂): Controls on Cu in the deep ocean. *Geochimica et Cosmochimica Acta*, **74**, 6721–6730.
- Statham P.J., Yeats P.A. and Landing W.M. (1998) Manganese in the eastern Atlantic Ocean: processes influencing deep and surface water distributions. *Marine Chemistry*, **61**, 55–68.
- Stone A.T. (1987) Reductive dissolution of manganese(III/IV) oxides by substituted phenols. *Environmental Science & Technology*, **21**, 979–988.
- Stone A.T. and Morgan J.J. (1984) Reduction and dissolution of manganese (III) and manganese(IV) oxides by organics. 1. Reaction with hydroquinone. *Environmental Science & Technology*, **18**, 450–456.
- Sunda W.G. and Huntsman S.A. (1990) Diel cycles in microbial manganese oxidation and manganese redox speciation in coastal waters of the Bahama Islands. *Limnology and Oceanography*, **35**, 325–338.
- Sunda W.G. and Huntsman S.A. (1994) Photoreduction of manganese oxides in seawater. *Marine Chemistry*, **46**, 133–152.
- Sunda W., Huntsman S. and Harvey G. (1983) Photoreduction of manganese oxides in seawater and its geochemical and biological implications. *Nature*, **301**, 234–236.
- Tamura N. and Cheniae G. (1987) Photoactivation of the water-oxidizing complex in Photosystem II membranes depleted of Mn and extrinsic proteins. I. Biochemical and kinetic characterization. *Biochimica et biophysica acta. Bioenergetics*, **890**, 179–194.
- Taylor S.R. (1964) Abundance of chemical elements in the continental crust: a new table. *Geochimica et Cosmochimica Acta*, **28**, 1273–1285.
- Tebo B.M., Bargar J.R., Clement B.G., Dick G.J., Murray K.J., Parker D., Verity R. and Webb S.M. (2004) Biogenic manganese oxides: Properties and mechanisms of formation. *Annual Review of Earth and Planetary Sciences*, **32**, 287–328.

- Tebo B.M., Johnson H.A., McCarthy J.K. and Templeton A.S. (2005) Geomicrobiology of manganese(II) oxidation. *Trends in Microbiology*, **13**, 421–428.
- Thenuwara A.C., Shumlas S.L., Attanayake N.H., Cerkez E.B., McKendry I.G., Frazer L., Borguet E., Kang Q., Zdilla M.J., Sun J. and Strongin D.R. (2015) Copper-intercalated birnessite as a water oxidation catalyst. *Langmuir*, **31**, 12807–12813.
- Thiagarajan N. and Lee C.T.A. (2004) Trace-element evidence for the origin of desert varnish by direct aqueous atmospheric deposition. *Earth and Planetary Science Letters*, **224**, 131–141.
- Turekian K.K. and Wedepohl K.H. (1961) Distribution of the elements in some major units of the Earth's crust. *Geological Society of America Bulletin*, **72**, 175.
- Turner S. and Buseck P. R. (1983) Defects in nsutite (γ -MnO₂) and dry-cell battery efficiency. *Nature*, **304**, 143–146.
- Villalobos M., Toner B., Bargat J. and Sposito G. (2003) Characterization of the manganese oxide produced by *Pseudomonas putida* strain MnB1. *Geochimica et Cosmochimica Acta*, **67**, 2649–2662.
- Villalobos M., Lanson B., Manceau A., Toner B. and Sposito G. (2006) Structural model for the biogenic Mn oxide produced by *Pseudomonas putida*. *American Mineralogist*, **91**, 489–502.
- Waite T.D., Wrigley I.C. and Szymczak R. (1988) Photoassisted dissolution of a colloidal manganese oxide in the presence of fulvic acid. *Environmental Science & Technology*, **22**, 778–785.
- Wang J.L., Li J.E., Jiang C.J., Zhou P., Zhang P.Y. and Yu J.G. (2017) The effect of manganese vacancy in birnessite-type MnO₂ on room-temperature oxidation of formaldehyde in air. *Applied Catalysis B – Environmental*, **204**, 147–155.
- Wang Q., Yang P. and Zhu M. (2018) Structural transformation of birnessite by fulvic acid under anoxic conditions. *Environmental Science & Technology*, **52**, 1844–1853.
- Wang Y. and Stone A.T. (2006a) The citric acid-Mn(III, IV) O₂ (birnessite) reaction. Electron transfer, complex formation, and autocatalytic feedback. *Geochimica et Cosmochimica Acta*, **70**, 4463–4476.
- Wang Y. and Stone A.T. (2006b) Reaction of Mn^{III, IV} (hydr) oxides with oxalic acid, glyoxylic acid, phosphonoformic acid, and structurally-related organic compounds. *Geochimica et Cosmochimica Acta*, **70**, 4477–4490.
- Wang Y., Feng X.H., Villalobos M., Tan W.F. and Liu F. (2012) Sorption behavior of heavy metals on birnessite: Relationship with its Mn average oxidation state and implications for types of sorption sites. *Chemical Geology*, **292**, 25–34.
- Webb S.M., Tebo B.M. and Bargat J.R. (2005) Structural characterization of biogenic Mn oxides produced in seawater by the marine bacillus sp. strain SG-1. *American Mineralogist*, **90**, 1342–1357.
- Wiechen M., Zaharieva I., Dau H. and Kurz P. (2012) Layered manganese oxides for water-oxidation: alkaline earth cations influence catalytic activity in a photosystem II-like fashion. *Chemical Science*, **3**, 2330–2339.
- Xu X.M., Ding H.R., Li Y., Lu A.H., Li Y. and Wang C.Q. (2018) Mineralogical characteristics of Mn coatings from different weathering environments in China: clues on their formation. *Mineralogy and Petrology*, **112**, 671–683.
- Xu X.M., Li Y., Li Y.Z., Lu A.H., Qiao R.X., Liu K.H., Ding H.R. and Wang C.Q. (2019) Characteristics of desert varnish from nanometer to micrometer scale: A photo-oxidation model on its formation. *Chemical Geology*, **522**, 55–70.
- Xu Y. and Schoonen M.A.A. (2000) The absolute energy positions of conduction and valence bands of selected semiconducting minerals. *American Mineralogist*, **85**, 543–556.
- Yang J., An H., Zhou X. and Li C. (2015) Water oxidation mechanism on alkaline-earth-cation containing birnessite-like manganese oxides. *Journal of Physical Chemistry C*, **119**, 18487–18494.
- Yang W.J., Zhu Y.F., You F., Yan L., Ma Y.J., Lu C.Y., Gao P.Q., Hao Q. and Li W.L. (2018) Insights into the surface-defect dependence of molecular oxygen activation over birnessite-type MnO₂. *Applied Catalysis B – Environmental*, **233**, 184–193.
- Yin H., Li H., Wang Y., Ginder-Vogel M., Qiu G., Feng X., Zheng L. and Liu F. (2014) Effects of Co and Ni co-doping on the structure and reactivity of hexagonal birnessite. *Chemical Geology*, **381**, 10–20.
- Yu D., Xu D., Zhao Z., Huang Q. and Zou S. (2020) Genesis of the Taolin Pb–Zn deposit in northeastern Hunan province, south China: constraints from trace elements and oxygen–sulfur–lead isotopes of the hydrothermal minerals. *Mineralium Deposita*, **55**, 1467–1488.
- Zhang C., Chen C., Dong H., Shen J.R., Dau H. and Zhao J. (2015) A synthetic Mn₄Ca-cluster mimicking the oxygen-evolving center of photosynthesis. *Science*, **348**(6235), 690–693.
- Zhang T., Liu L., Tan W., Suib S.L., Qiu G. and Liu F. (2018) Photochemical formation and transformation of birnessite: effects of cations on micromorphology and crystal structure. *Environmental Science & Technology*, **52**, 6864–6871.
- Zhu M., Ginder-Vogel M. and Sparks D.L. (2010) Ni(II) sorption on biogenic Mn-oxides with varying Mn octahedral layer structure. *Environmental Science & Technology*, **44**, 4472–4478.
- Zwicker W.K., Groeneveld Meijer W.O.J. and Jafee H.W. (1962) Nsutite – a widespread manganese oxide mineral. *American Mineralogist*, **47**, 246–266.